STOCHASTIC SYNCHRONY AND PHASE RESETTING CURVES: THEORY AND APPLICATIONS

by

Sashi K. Marella

B.S., Purdue University 2003,

M.S., Purdue University, 2005.

Submitted to the Graduate Faculty of

the Center for Neuroscience in partial fulfillment

of the requirements for the degree of

Doctor of Philosophy

University of Pittsburgh

2012

UNIVERSITY OF PITTSBURGH

DIETRICH SCHOOL OF ARTS AND SCIENCES

This dissertation was presented

by

Sashi K. Marella

It was defended on

May 2nd 2011

and approved by

Bard Ermentrout, Department of Mathematics

Nathan Urban, Department of Biology, Carnegie Mellon University

Brent Doiron, Department of Mathematics

William Troy, Department of Mathematics

Rob Kass, Department of Statistics, Carnegie Mellon University

Xiao-Jing Wang, Department of Neurobiology, Yale University

Dissertation Director: Bard Ermentrout, Department of Mathematics

ABSTRACT

STOCHASTIC SYNCHRONY AND PHASE RESETTING CURVES: THEORY AND APPLICATIONS

Sashi K. Marella, PhD

University of Pittsburgh, 2012

We investigate the relationship between the shape of the phase-resetting curve (PRC) and the degree of stochastic synchronization observed between a pair of uncoupled general oscillators receiving partially correlated Poisson inputs. Using perturbation methods, we derive an expression relating the shape of the PRC to the probability density function (PDF) of the phase difference between the oscillators. Using various measures of synchrony and cross-correlation we demonstrate that the degree of stochastic synchronization is dependent on the firing rate of the neuron and the membership of the PRC (Type I or Type II). We apply our theory to the olfactory bulb to investigate whether the correlated output of the olfactory bulb granule cells can synchronize uncoupled mitral cells via a positive feedback loop in correlation. We demonstrate the emergence and temporal evolution of input correlation in recurrent networks with feedback. We also investigate the rate of convergence to the steady-state PDF using an analytical approach. Our investigation explores several theoretical models ranging from spiking models to abstract analytically tractable models.

Keywords: Phase resetting curve, Stochastic synchronization, Correlation, Synchrony, Recurrent networks.

TABLE OF CONTENTS

LIST OF FIGURES

1.0 INTRODUCTION

In this thesis we study the phenomenon of stochastic synchronization between uncoupled oscillators using theoretical analysis and computer simulations. We then use our theoretical results to investigate the mechanism of synchronization of principal neurons in the olfactory bulb. In this chapter we provide a background of the various biological and theoretical aspects of the problem.

- 1.1 In this section we provide a brief introduction to the olfactory system and the motivation to study networks with mitral and granule cells where the only type of coupling present is the mitral-granule reciprocal dendrodenritic synapse.
- 1.2 In this section we provide an overview on synchrony in the nervous system. We also discuss some mechanisms of synchrony that are germane to our investigation.
- 1.3 In this section we introduce the phase resetting curve.

1.1 OLFACTORY BULB

Olfaction is an important mode of gathering sensory information from the environment employed by living organisms on this planet. This is especially significant in the case of mammals, fish and insects which have a highly developed sense of smell. Odorant molecules can carry information about predators, prey, and reproductive opportunities which are critical environmental parameters that an organism must be aware of, in order to maximize its survival. Olfaction begins with the entry of odorant molecules into the nostrils. These molecules travel through the nasal canal and get embedded in a layer of mucus secreted by

the nasal epithelium. Here, these molecules may bind to odorant receptors expressed by olfactory receptor/sensory neurons on hair-like cilia on their dendritic membranes. Upon binding a ligand, the receptor transduces the signal via secondary messenger pathways resulting ultimately in the generation of an action potential in the receptor neuron.

Multiple axons of olfactory receptor neurons travel further up together as olfactory nerves through a sieve-like bone called the cribiform-plate into the olfactory bulb. In the olfactory bulb, the axons terminate in spherical structures called glomeruli. These glomeruli also harbor the apical dendrites of cells called mitral cells. Mitral cells are the principal excitatory neurons of the olfactory bulb. Their apical dendrites receive incoming odor information from the olfactory receptor neurons and their axons project to the piriform cortex, entorhinal cortex and the amygdala. The major inhibitory neurons in the olfactory bulb are the granule cells discovered by Camillo Golgi in the year 1875 [37, 85]. The existence of spines on granule cell dendrites were proved by Ramon y Cajal [12]. Mitral cells in addition to their apical/primary dendrites in the glomerulus also have basal/secondary dendrites. The existence of reciprocal dendrodenritic connections between the basal dendrites of mitral cells and the dendrites of granule cells was supported by experimental and theoretical studies [42, 76, 75] before it was definitively described [73, 74].

The basal dendrites of mitral cells can extend laterally for long distances onto neighboring glomeruli [84]. This suggests that distant mitral cells may be synaptically coupled. But, although there have been some studies indicating the existence of direct, electrical, dendritic, excitatory mitral cell coupling [47, 14, 81, 98] between glomerular-specific mitral cells, such coupling between glomerular-non-specific mitral cells has not been clearly demonstrated. On the other hand, recent experimental studies have suggested that the laterally extended morphology of the basal dendrites of mitral cells could potentially activate granule cells situated as far as 1 mm away. This distance was estimated by recording the distance to which a full action potential invades the basal dendrites [107]. Viral tracer experiments have revealed that granule cells exist in widely distributed clusters [106]. Narrow clusters of granule cells have been observed to be centered around each glomeruli and it has been suggested that these narrow clusters of granule cells along with mitral cells form a 'glomerular unit column'. These properties of neurons in the olfactory bulb suggests that mitral-granule

interactions are an important feature of the olfactory bulb.

1.2 SYNCHRONY

Synchrony is a universal concept. Although humans understand the intuitive concept of synchrony, academic interest in synchrony might have been set in motion in the $1700's$ when Christiaan Huygens made the observation that pendulums hung on the same wall tend to synchronize with each other [71]. In 1727, Jean-Jacques d'Ortous de Mairan found experimental evidence for circadian rhythms in plants. In neuroscience, synchrony gained prominence after recordings of electrical activity in the fish olfactory organs showed synchronous discharges of electrical activity [4]. Similar synchronous discharges were later observed in the hedgehog [2]. More recently, it was shown that action potentials generated by cortical cells can align with the oscillatory rhythm which results in phase-locking of neuronal firing to synchronized oscillations [40, 41, 17]. It was also proposed [39] that gamma frequency synchronization between cell assemblies can promote integration of sensory information. Synchrony can influence transmission of activity from one group of neurons to another [94, 77]. Also, synchronous presynaptic neurons with common postsynaptic targets can effectively depolarize the postsynaptic neurons which leads to a more efficient mode of propagating spiking information to downstream targets [79, 64].Synchronous oscillations are grouped into discrete frequency ranges,beta(15-30),theta(4-8),gamma(30-80) etc. The olfactory bulb has long been known for its robust gamma rhythms [2, 3, 10, 83, 18]. Since the olfactory bulb is our prime focus we will discuss the mechanisms to generate gamma rhythms.

1.2.1 Mechanisms of Gamma synchrony

1.2.1.1 Interneuron Network Gamma (ING) Cortical GABAergic neurons show a high degree of mutual connectivity [90], therefor it is not surprising that most inhibitory neurons form networks. The ING mechanism was first experimentally investigated by [105, 95]. In these experiments, excitatory synaptic transmission was blocked using AMPA and NMDA

channel blockers while simultaneously activating the metabotropic glutamate receptors. Metabotropic glutamate receptor activation depolarizes the inhibitory neuron population. It was observed that intracellular recordings from pyramidal cells revealed a highly synchronous barrages of IPSP's onto the pyramidal cells in the frequency range of 30-50 Hz. The ING mechanism requires that at least a fraction of the individual interneurons have firing frequencies higher than the frequency of the population rhythm [96, 105, 101]. If such a network is excited, the resulting population rhythm will be governed by the timecourse of inhibition from one neuron to another [105, 96, 101] which includes the timecourse of the IPSP and after-hyperpolarization currents if present. With slower synapses, it has been shown that the mechanism of synchronization of a coupled neurons is by the "Escape scenario" where the coupled neurons can all fire action potentials and undergo inhibition together resulting in population synchrony [102].

In the Wang-Buzsaki model, manipulating the firing frequency or changing the strengths of synapses does not prevent the generation of the highest synchrony at gamma frequencies [101]. The coherence of the Wang-Buzsaki model does break down with heterogeneities but the decrease is least when the network parameters allow the system to synchronize in the gamma range [101]. In order to overcome heterogeneities, the conductance of the GABA synapse should be large [99, 6]. The ING mechanism is most robust to heterogeneities when the decay constant of the IPSP matches the period of oscillation [101]. Theoretical investigations have supported these findings by showing that homogeneous networks can synchronize in a wider range of frequencies [100]. The proposed mechanism of synchronization is based on mutual coupling of interconnected network of inhibitory neurons. These neurons receive identical inputs which results in all the neurons firing together. If some fraction fires at the wrong time, they receive inhibition from the majority of the synchronized neurons. This inhibition delays their next spike and after a few cycles of successive spike delay allows them to synchronize with the rest of the population.

1.2.1.2 Pyramidal Interneuron Network Gamma (PING)

PING was proposed to explain the data obtained by researchers in the mid-nineties. These workers reported robust recruitment of pyramidal cells during oscillatory activity. The first group used tetanic

stimuli and metabotropic glutamate receptor activators [104] while the second group used the cholinergic agonist carbachol [28]. Since pyramidal neurons are recruited in this type of oscillatory activity, the excitatory neuron population will be able to modulate the activity of the interneuron network via feed back excitation. This sets up an oscillation involving the interplay between interneurons and excitatory neurons. Excitatory neuronal firing generates EPSPs that seem to play a role in stabilizing the network oscillation. It has been shown that drugs like diazepam and thiopental decrease the oscillation frequency to a greater extent for ING compared to when pyramidal cells were participating in the network oscillation [103]. The importance of inhibitory neurons was highlighted recently in two experiments using Channelrhodopsin and Halorhodopsin to optically depolarize and hyperpolarize neurons. Depolarization of cortical inhibitory cells caused an increase in the frequency of oscillations and hyperpolarizing them caused a decrease in the oscillation frequency [88]. When inhibitory cells were driven by random light pulses, the gamma peak was distinctly enhanced compared to other frequency bands [13]. When periodic light pulses were used, it was found that the pulses were more effective at eliciting gamma oscillations when directed toward the interneuron population compared to the excitatory neuronal population [13]. EPSPs can also facilitate spatially separated cortical areas to oscillate in the gamma range with a small phase difference. This was analyzed by [26] using maps which shed light on the role of the doublet spike in synchronizing spatially separated cortical areas. In general, interneurons in ING networks should have sufficient drive to overcome inhibition and fire action potentials. In this case the excitatory cell fires when the level of noise is low. Alternatively, ING networks may receive external drive to its excitatory neurons such that it is barely enough for the excitatory neurons to fire once every cycle but only after the inhibitory cells fire. In an ideal PING network, the excitability of the excitatory population should be such that the excitatory neurons recover from inhibition faster than interneurons thus allowing them to activate the interneuronal population to start the next cycle. It has also been shown that active involvement of the excitatory neurons in the network [96, 101] makes it less vulnerable to heterogeneities.

1.2.1.3 Stochastic synchrony

Stochastic synchrony was first proposed [63] as a mechanism to explain an observation that there were spatial correlations in the cycles of fur returns of Canadian lynx [19]. Now, it is a frequently studied subject in neuroscience and applied mathematics [31, 32, 33, 66, 71, 93, 16, 15, 1, 27, 61, 60]. The mechanism allows for synchronization of uncoupled oscillators receiving partially correlated noisy inputs. In the olfactory bulb, it recently been proposed that generation of gamma oscillations could occur via such a stochastic process rather than via PING. We will say more about this mechanism later.

1.3 PRC

In this section we introduce the phase resetting curve. PRC's are an indispensable tool that describes the response of an oscillator to an external input at a given phase during its oscillation. Let us consider a differential equation in R^n

$$\frac{dX}{dt} = F(X). \tag{1.1}$$

If we suppose that this system has an asymptotically stable limit cycle Γ which has a period T. Asymptotic stability implies that nearby initial conditions approach Γ as $t \to \infty$ We can parametrize Γ with respect to the period T and define a phase, $\theta \in [0, T)$, along the limit cycle. Let $\Phi(x)$ be the phase of the oscillator for a point x on Γ. Since the limit cycle is asymptotically stable, it is possible to define a phase for points y in the neighborhood of the cycle. Then we can define $\Phi(y) = \Phi(x)$ where $\Phi(x)$ is the asymptotic phase of y, i.e. $\|X(t; x) - X(t; y)\| \to 0$ as $t \to \infty$. The set of points y which have the same asymptotic phase is called the isochron of the limit cycle. An external perturbation given at phase ϕ can move the system to a different isochron where the new phase is ϕ'. The phase resetting curve is defined as the difference between the new phase and the old phase.

$$\Delta(\phi) = \phi' - \phi \tag{1.2}$$

1.4 MOTIVATION

1.5 OUR THEORETICAL RESULTS

Galan et al [33] showed that olfactory principal neurons can undergo partial synchronization when driven by partially correlated synaptic inputs. There is a fundamental difference between Class-I and Class-II excitable neurons in their response to external inputs. Class-I neurons tend to undergo a phase advance owing to their positive PRCs. Class-II neurons on the other hand can be advanced or delayed in phase in response to an input. In addition, neurons in the olfactory cortex exist in recurrent networks. It is not clear whether and how feedback affects the stochastic synchronization properties of these neurons. In order to understand the response of principal neurons in the olfactory bulb to correlated noise we have to investigate the case where input correlation is not fixed. In addition, the rate of convergence to a steady-state density of phase differences for stochastic synchronization remain unknown.

1.5.1 Thesis goals and Results

The main goals of this thesis are

- (I) To obtain a closed-form expression for the relationship between the PRC and the steady-state density of phase differences for two uncoupled oscillators receiving partially correlated inputs.
- (II) To investigate the effects of feedback on a network of neurons undergoing stochastic synchronization.
- (III) To obtain an expression for the rate of convergence to the steady-state density of phase differences.

Our main results are

- (I) We obtain a closed-form expression for the relationship between the PRC and the steady-state density of phase differences.

- (II) We show that feedback causes an amplification of correlation via a positive feedback loop in correlation.

- (III) We obtain an expression for the rate of convergence for the system of coupled oscillators without feedback.

1.6 CHAPTER OUTLINES

1.6.1 Chapter 2: Stochastic synchronization and the Phase resetting curve

In this chapter we analyze a system of phase oscillators receiving partially correlated inputs. Using perturbation methods, we obtain a closed-form solution for the steady-state density of phase differences. We then define order parameters for synchrony and cross-correlation and use these order parameters to quantify the degree of stochastic synchronization in this system of oscillators. We also study the effect of firing rates in a Morris-Lecar system on the degree of stochastic synchronization. Additionally, we use the order parameters to quantify other frequently used models like the leaky integrate-and-fire model and the Wang-Buzsaki interneuron model.

1.6.2 Chapter 3: Amplification of stochastic synchronization in recurrent networks

In this chapter we investigate a spiking neuron model with feedback to qualitatively demonstrate the emergence of self-organized synchrony. Then we use an abstract model to obtain an expression for the averaged dynamics and compare our predicted solutions for fixed points with those obtained using Monte-Carlo simulations. We also show that the choice of the functional Γ in equation 3.4 affects the stability of the fixed points. Specifically, we address the mechanism by which bistability could arise in the system.

1.6.3 Chapter 4: Rate of convergence of stochastic synchrony

In this chapter we obtain an expression for the rate of convergence to the steady-state density of phase differences in a two oscillators system receiving partially correlated inputs without feedback. We use the closed-form expression obtained from chapter 2 to obtain an approximation using the perturbation technique suited for computing large eigenvalues. Our theoretical values show a close match to values obtained through simulation.

2.0 STOCHASTIC SYNCHRONIZATION AND THE PHASE RESETTING CURVE

2.1 INTRODUCTION

There has recently been a great deal of interest in the ability of noise to synchronize limit cycle oscillators even when they are uncoupled [72, 93, 36, 46, 108, 57, 69, 58]. Two uncoupled limit cycle oscillators driven by partially or fully correlated noise that is not too strong are able to synchronize in the sense that their phase difference approaches a stationary distribution peaked around zero. Goldobin et al [36] and more recently Nakao et al [66] derived expressions for the density of phase-differences when oscillators are driven by partially correlated white noise. In recent experiments, Galan et al [33] showed partial synchronization of two olfactory bulb neurons when driven by partially correlated synaptic events. If this so-called stochastic synchronization plays a role in biological networks, then it would be useful to quantitatively characterize the consequences of uncorrelated signals and oscillator heterogeneity as a function of the details of the oscillators. For small noise levels, it has been shown [36, 66, 93] (for white noise stimuli) that a general limit cycle oscillator can be reduced to a scalar equation for the phase characterized by the phase-resetting curve or PRC. The PRC of an oscillator describes how the timing of a brief signal changes the phase of the oscillator. PRCs are easily measured experimentally and computed numerically for a given model.

Neural and other biological oscillators can be classified broadly into two types based on their intrinsic dynamics [78]. That is, as a parameter changes (e.g., the injected current in a neuron), the system goes from a stable rest state to periodic firing through a bifurcation; two such bifurcations characterize the majority of tonically spiking neurons. Class I excitable

neurons undergo *saddle-node on invariant circle* bifurcations and can theoretically fire at arbitrarily low finite frequencies whereas Class II excitable neurons undergo either *sub-* or *super-critical Andronov-Hopf* bifurcations and possess a non-zero minimum frequency of firing. Ermentrout and collaborators [23, 43], Hansel et al [44] and more recently Brown et al [11] have demonstrated that there is a strong connection between the bifurcation class of a neuron and the shape of its phase-resetting curve. Class I excitable neurons, at least near the bifurcation, tend to have PRCs which are non-negative; inputs can only advance the phase [21]. Class II excitable neurons tend to have PRCs which have both positive and negative parts [21]. Thus for class II excitable neurons, the next spike is advanced or delayed depending on the timing of the subthreshold input. The shape of the PRC plays an important role in determining whether coupled neurons are able to synchronize both in models [38, 22, 23, 43, 31] and in experimentally manipulated neurons [35, 59, 67] . Thus, we expect that the shape of a neural PRC might also factor in the degree of stochastic synchronization to noise. Recently, Tateno and Robinson [92, 91] used the phase resetting curve of both model neurons and cortical neurons to study how the shape of the PRC affects the rate that two identical neurons driven by perfectly correlated noise can synchronize. Galan et al [32] used finite element method to contrast the stochastic synchronization of class I and class II neurons to white noise. Interestingly, Tsubo et al [97] show that the shape of the PRCs is different in different layers of the rat motor cortex.

In this paper, we first derive an expression for the density of phase-differences for two identical oscillators driven by partially correlated Poisson inputs. It turns out that in the limit of small perturbations, we obtain a result identical to Nakao's recent calculation [66]. Secondly, we explore how the shape of the PRC impacts the relationship between the input correlation and synchrony of driven oscillators. Finally, we explore the effects of the oscillator frequency on stochastic synchrony as it is known ([43]) that frequency has a strong effect on the shape of the PRC.

2.2 DERIVATIONS

2.2.1 Reduction to a phase equation

Consider a general limit-cycle oscillator that is driven by an input:

$$\frac{dX}{dt} = F(X(t)) + G(X(t), t)$$

When $G = 0$, we have a stable periodic solution, $X_0(t)$. As in Kuramoto [53], we can introduce a phase variable along limit cycle, θ so that we write $X(t) = X_0(\theta(t))$ and obtain

$$\frac{d\theta}{dt} = 1 + Z(\theta(t)) \cdot G(X_0(\theta(t)), t)$$

as long as G is small (which is the case we consider here). The vector function, $Z(\theta)$ describes the phase-shift of the oscillator as a function of the timing (phase) of the stimulus. Now suppose that $X(t)$ is a neural oscillator which is driven by a series of pulsatile inputs with amplitude a_m at times $t_1, t_2, \ldots$. Since the drive only appears in the voltage variable, only the voltage component of $Z(\theta)$ matters; this is the infinitesimal phase resetting curve $\Delta(\theta)$ for the neuron. Thus the phase satisfies:

$$\frac{d\theta}{dt} = 1 + \sum_m \Delta(\theta(t)) a_m \delta(t - t_m).$$

Let $\tau_m = t_m - t_{m-1}$ be the time between impulses. Between inputs, the phase (measured in units of time) advances by τ_m, If we let θ_m be the phase right before the m^{th} stimulus, then

$$\theta_{m+1} = \theta_m + \tau_m + a_m \Delta(\theta_m). \tag{2.1}$$

We note that θ lies between $[0, T)$ where T is the natural period of the oscillator. We now have reduced the driven oscillator to a one-dimensional map. If the pulsatile stimuli are not delta functions but rather some type of brief synaptic current, then the map derivation can be valid (or certainly a good approximation) when the PRC is replaced by another quantity called the spike-time response curve (STRC, S(θ)). For example if the inputs are time-dependent functions, say, $i(t)$, then the PRC is replaced by:

$$\mathrm{S}(\theta) = \int_0^\infty \Delta(\theta - \theta') i(\theta') \, d\theta'.$$

With regular inputs, this replacement is valid as long as $i(t)$ lasts for a short time compared to the interstimulus interval. However, for Poisson inputs, the interstimulus interval can be arbitrarily short, so that using an STRC may not be formally legitimate.

Experimentally, the function $\Delta(\theta)$ is obtained by perturbing the oscillator with small stimuli (say, amplitude a) and measuring the change in the spike-time:

$$\widehat{\Delta}(t,a) \equiv T - T_{pert}(t,a).$$

The function $\Delta(t)$ is defined as

$$\Delta(t) = \lim_{a\to 0} \frac{\widehat{\Delta}(t,a)}{a}.$$

It is called the *infinitesimal PRC*. For numerically computed oscillations, $\Delta(t)$ is found by solving the adjoint equation, a linear equation associated with the limit cycle solution [25].

2.2.2 Phase Distribution Equation

We first consider the invariant phase of a single perturbed oscillator. If τ_m are taken from a distribution, $Q(\tau)$ ($\tau \in [0,T)$) and a_m are taken from a distribution with density, $f(a)$, then we can readily derive an equation for the density of phases, θ_m, in equation (2.1) using methods of Lasota and Mackey [56] . Let $P_m(\theta)$ be the density of θ_m. Then

$$P_{m+1}(\theta) = \int_{-\infty}^{\infty}\int_0^T P_m(y)Q(\theta - y - a\Delta(y))f(a)\ dy\ da.$$

A number of authors have analyzed this model when $f(a)$ is strongly peaked near $a = 0$, e.g., stimuli are weak; or when the Poisson rate is very fast. Nakao et al [65] and Ermentrout et al [24] show that to lowest order, the invariant density, $\varphi(\theta) \equiv P_\infty(\theta)$ is very close to uniform, $\varphi(\theta) \approx 1/T$. We will show later, that formally, we have to make a small correction even for weak inputs, but for Poisson inputs at low rates, the results are indistinguishable from those obtained by treating $\varphi(\theta)$ as uniform. For notational simplicity, we will assume that the period, T has been scaled to 1. Consider, now, N identical uncoupled oscillators, driven with pulsatile stimuli that are only partially shared. That is, at any given moment, some oscillators will receive a perturbation, but others will not. Our goal is to study how synchronous the oscillators are as a function of the degree of sharing. As the oscillators are

uncoupled, it suffices to analyze a pair. Thus, consider two such oscillators with identical periods:

$$\Theta_{n+1} = \Theta_n + \tau_n + \epsilon a_n \Delta(\Theta_n) \tag{2.2}$$

$$\Psi_{n+1} = \Psi_n + \tau_n + \epsilon b_n \Delta(\Psi_n) \tag{2.3}$$

where Θ and Ψ denote the phase of the oscillators at the time of the n^{th} input. τ_n is the period of stimulation, specifically it is the time between the n^{th} and the $n+1^{th}$ inputs and is assumed here to be a Poisson variable. The parameter, ϵ scales the magnitude of the perturbations. We allow for heterogeneity in the inputs; some inputs are shared while others are not. The easiest way to do this is to assume that a_n, b_n are either 0 or 1: $(a_n, b_n) \in \{(1,1),(0,1),(1,0)\}$ with probabilities $q, (1-q)/2$ and $(1-q)/2$ respectively. Thus, q is the probability that both oscillators receive the same input and thus is related to the correlation of the inputs. In section2.5 we show that the correlation is, $c := 2q/(q+1)$. Additional heterogeneity could come via small differences in the frequencies of the oscillators. At the end of the derivation, we discuss this point briefly. We assume Δ to be a periodic function with period 1. The phase difference of the oscillators at the time of the $n+1^{th}$ input, $\delta_n = \Theta_n - \Psi_n$ can be obtained by subtracting equation (2.3) from (2.2).

$$\delta_{n+1} = \delta_n + \epsilon \left(a_n \Delta(\delta_n + \Psi_n) - b_n \Delta(\Psi_n) \right).$$

In order to analyze these equations, we will derive an equation for the density of δ_n using methods for stochastic maps in [56]. We note that Ψ_n are random variables which are independent of δ_n and furthermore, that a_n and Ψ_n are independent as well since Ψ_n depends only on a_{n-1}. Thus, given the probabilities of a_n, b_n and Ψ_n, we can compute the evolution of the density for δ_n and thus the invariant density.

Let $p_n(x)dx := \Pr(\delta_n \in [x, x+dx))$, that is, $p_n(x)$ is the density function for the phase difference, δ_n. With some abuse of notation, we will suppress the dx, first on the RHS and later on the LHS of the definition. Let

$$E[U(\Psi)] := \int_0^1 U(\Psi)\varphi(\Psi)\, d\Psi$$

where U is an arbitrary function of Ψ and $\varphi(\Psi)$ is the invariant density for Ψ_n. Henceforth, we drop the subscript n from Ψ_n.

$$\begin{aligned} p_{n+1}(x)dx &= E[\Pr(\delta_n + \epsilon a_n \Delta(\delta_n + \Psi) - \\ &\qquad \epsilon b_n \Delta(\Psi) = x)] \\ &= qE[p_n^{11}(x,\Psi)dx] \\ &\quad + \left(\frac{1-q}{2}\right)(E[p_n^{01}(x,\Psi)dx] + \\ &\qquad E[p_n^{10}(x,\Psi)dx]) \end{aligned}$$

where $p_{n+1}^{ab}(x,\Psi)dx$ is the probability that $\delta_{n+1} = x$ given (a,b) and Ψ. We now compute all the $p_n^{ab}(x,\Psi)dx$ quantities.

$$\begin{aligned} p_n^{01}(x,\Psi)dx &= \Pr(\delta_n - \epsilon\Delta(\Psi) = x) \\ &= \Pr(\delta_n = \epsilon\Delta(\Psi) + x) \\ &= p_n(\epsilon\Delta(\Psi) + x)dx. \end{aligned}$$

Before continuing, we define $F(x) := x + \epsilon\Delta(x)$. For ϵ sufficiently small, $F(x)$ is an invertible function.

$$\begin{aligned} p_n^{10}(x,\Psi)dx &= \Pr(\delta_n + \epsilon\Delta(\delta_n + \Psi) = x) \\ &= \Pr(\delta_n + \Psi + \epsilon\Delta(\delta_n + \Psi) = x + \Psi) \\ &= \Pr(F(\delta_n + \Psi) = x + \Psi) \\ &= \Pr(\delta_n = F^{-1}(x + \Psi) - \Psi). \end{aligned}$$

Since,

$$\begin{aligned} \Pr(\delta_n + \epsilon\Delta(\delta_n + \Psi) \le x) &= \Pr(F(\delta_n + \Psi) - \Psi \le x) \\ &= \Pr(\delta_n \le F^{-1}(x + \Psi) - \\ &\qquad \Psi). \end{aligned}$$

We can write,

$$\begin{aligned} p_n^{10}(x,\Psi) &= \frac{d}{dx}\int_0^x p_n^{10}(s,\Psi)\, ds \\ &= \frac{d}{dx}\int_0^{F^{-1}(x+\Psi)-\Psi} p_n(s,\Psi)\, ds \\ &= p_n(F^{-1}(x+\Psi) - \Psi, \Psi).\frac{d}{dx}(F^{-1}(x+\Psi) - \\ &\qquad \Psi) \\ &= \frac{p_n(F^{-1}(x+\Psi) - \Psi, \Psi)}{F'(F^{-1}(x+\Psi))}. \end{aligned}$$

Hence, $p_n^{10}(x,\Psi)dx = \dfrac{p_n(F^{-1}(x+\Psi)-\Psi,\Psi)dx}{F'(F^{-1}(x+\Psi))}$.

Lastly,

$$\begin{aligned} p_n^{11}(x,\Psi)dx &= \Pr(\delta_n + \epsilon(\Delta(\delta_n+\Psi)-\Delta(\Psi)) = x) \\ &= \Pr(\delta_n + \Psi + \epsilon\Delta(\delta_n+\Psi) = x+\Psi+ \\ &\qquad\qquad \epsilon\Delta(\Psi)) \\ &= \Pr(F(\delta_n+\Psi) = x + F(\Psi)) \\ &= \Pr(\delta_n = F^{-1}(x+F(\Psi))-\Psi) \\ &= \frac{p_n(F^{-1}(x+F(\Psi))-\Psi),\Psi)dx}{F'(F^{-1}(x+F(\Psi)))}. \end{aligned}$$

Thus, $p_n(x)$ satisfies the Frobenius-Perron equation:

$$\begin{aligned} p_{n+1}(x) &= \int_0^1 \varphi(\Psi) q p_n^{11}(x,\Psi)dx \\ &\quad + \left(\frac{1-q}{2}\right)[p_n^{10}(x,\Psi)dx + \\ &\qquad\qquad p_n^{01}(x,\Psi)dx]\; d\Psi \end{aligned}$$

The invariant (steady-state) density is found by equating $p_n(x)$ and $p_{n+1}(x)$, thus we need to solve

$$\begin{aligned} p(x) = \int_0^1 \varphi(\Psi) &\left[q\left(\frac{pF^{-1}(x+F(\Psi)-\Psi))}{F'(F^{-1}(x+F(\Psi)))}\; d\Psi\right)\right. \\ &+\left(\frac{1-q}{2}\right)\left(\frac{p(F^{-1}(x+\Psi)-\Psi))}{F'(F^{-1}(x+\Psi))}\right. \\ &\qquad \left.\left. +p(\Delta(\Psi)+x)\right)\right] \end{aligned} \tag{2.4}$$

In order to analyze equation (2.4), we need to know the distribution of the phase, $\varphi(\Psi)$. As noted at the beginning of this section, if the stimuli are small, that is, $\epsilon \ll 1$, then $\varphi(\Psi) \approx 1$; it is very close to uniform. In this case, the integrals in equation (2.4) are simple averages. However, as our calculations for the invariant density, $p(x)$ require $O(\epsilon^2)$ terms, we have to compute $\varphi(\Psi)$ up to order ϵ. The uniform approximation has been used in other papers, but, strictly speaking, we need to include the next order terms. As we will see later

on, the higher order terms in $\varphi(\Psi)$ make almost no difference for Poisson inputs at low rates. In the section 2.6, we derive the expression for $\varphi(\Psi)$ for Poisson inputs with rate r:

$$\varphi(\Psi) = 1 - \epsilon\big(r\frac{1+q}{2}\left(\Delta(\Psi) - \bar{\Delta}\right)\big) \tag{2.5}$$

where $\bar{\Delta}$ is the average of $\Delta(\Psi)$.

Now, let $y = F(x) = x + \epsilon\Delta(x)$ and express x approximately in terms of y.

$$x \approx y + \epsilon y_1 + \epsilon^2 y_2$$

$$\begin{aligned} \Rightarrow F(x) &= x + \epsilon\Delta(x) \\ &\approx y + \epsilon y_1 + \epsilon^2 y_2 + \epsilon\Delta(y + \epsilon y_1 + \epsilon^2 y_2). \end{aligned}$$

By Taylor expansion of $\epsilon\Delta(y + \epsilon y_1 + \epsilon^2 y_2)$ around y we get

$$\begin{aligned} \epsilon\Delta(y + \epsilon y_1 + \epsilon^2 y_2) &\approx \epsilon\Delta(y) + \epsilon^2\Delta'(y)y_1 + O(\epsilon^3) \\ \Rightarrow F(x) &\approx y + \epsilon y_1 + \epsilon^2 y_2 + \epsilon\Delta(y) + \epsilon^2\Delta'(y)y_1. \end{aligned}$$

Equating the ϵ terms we can solve for y_1 and y_2 obtaining the inverse to second order:

$$x = F^{-1}(y) \approx y - \epsilon\Delta(y) + \epsilon^2\Delta'(y)\Delta(y) \tag{2.6}$$

We use the result in (2.6) to express terms in (2.4) in terms of their expansion in ϵ. For example, a term like $p(F'(F^{-1}(g)))$ (which does not appear in (2.4)) can be expressed using (2.6) as

$$p(F'(F^{-1}(g))) = p(1 + \epsilon\Delta'(x(g - \epsilon\Delta g) + \epsilon^2\Delta' g\Delta g))$$

leading to

$$\begin{aligned} &p(1) + \epsilon p'(1)\Delta'(g) \\ &\quad + \epsilon^2\left(-p'(1)\Delta''(g)\Delta(g) + \tfrac{1}{2}p''(1)\Delta(g)^2\right) \\ &\quad + O(\epsilon^3). \end{aligned}$$

Using the above scheme, (2.4) can be expressed as

$$
\begin{aligned}
p(x) \;=\; & \int_0^1 [1+\epsilon\varphi_1(\Psi)]\Bigg[q\Bigg[p(x)+\epsilon\Big(-p'(x)(-\Delta(\Psi)+\Delta(x+\Psi))-p(x)\Delta'(x+\Psi)\Big)\\
& +\epsilon^2\Big(-p'(x)\Delta'(x+\Psi)\Delta(\Psi)+p'(x)\Delta'(x+\Psi)\Delta(x+\Psi)+\frac{1}{2}p''(x)(\Delta(\Psi))^2\\
& -p''(x)\Delta(\Psi)\Delta(x+\Psi)+1/2\,p''(x)(\Delta(x+\Psi))^2+p(x)\Delta''(x+\Psi)(-\Delta(\Psi)+\\
& \Delta(x+\Psi))+(-p'(x)\Delta(\Psi)+p'(x)\Delta(x+\Psi)+p(x)\Delta'(x+\Psi))\Delta'(x+\Psi)\Big)\\
& +O(\epsilon^3)\Bigg]
\end{aligned}
$$

$$
\begin{aligned}
+\frac{1-q}{2} \;\; & \Bigg[p(x)+\epsilon\Big(-p'(x)\Delta(x+\Psi)-p(x)\Delta'(x+\Psi)\Big)\\
& +\epsilon^2\Big(p'(x)\Delta'(x+\Psi)\Delta(x+\Psi)+\frac{1}{2}p''(x)(\Delta(x+\Psi))^2\\
& +p(x)\Delta''(x+\Psi)\Delta(x+\Psi)+(p'(x)\Delta(x+\Psi)+p(x)\Delta'(x+\Psi))\Delta'(x+\Psi)\Big)\\
& +O(\epsilon^3)\Bigg]\\
+\frac{1-q}{2} \;\; & \Bigg[p(x)+\epsilon p'(x)\Delta(\Psi)+\frac{1}{2}\epsilon^2 p''(x)(\Delta(\Psi))^2+O(\epsilon^3)\Bigg]\Bigg]\; d\Psi.
\end{aligned}
$$

To lowest order, we get

$$p(x)=\int_0^1 p(x)\; d\Psi = p(x).$$

To order ϵ, we obtain

$$0=qp(x)\int_0^1 \varphi_1(\Psi)d\Psi+\frac{q+1}{2}\int_0^1 \; p'(x)\Delta(\Psi)-p'(x)\Delta(x+\Psi)-p(x)\Delta'(x+\Psi)\; d\Psi.$$

Since $\varphi(\Psi)$ is the invariant density, by definition $\int_0^1 \varphi(\Psi)d\Psi = 1$. Hence $\int_0^1 \varphi_1(\Psi)d\Psi$ =0, where φ_1 is the 1^{st} order ϵ term in the expansion of $\varphi(\Psi)$ (see section 2.6). Hence we can write,

$$
\begin{aligned}
0 \;\; = & \frac{q+1}{2}\int_0^1 \; p'(x)\Delta(\Psi)-p'(x)\Delta(x+\Psi)\\
& -p(x)\Delta'(x+\Psi)\; d\Psi.
\end{aligned}
$$

Using the periodicity of $\Delta(\Psi)$, we observe that the right hand side is zero independent of $p(x)$. Henceforth, we denote $p(x)$ as p for reasons of brevity. To second order we must have :

$$\begin{aligned}
0 = \int_0^1 \Big(& -4qp'\Delta'(x+\Psi)\Delta(\Psi) + 2qp'\Delta'(x+\Psi)\Delta(x+\Psi) \\
& + \frac{1}{2}qp''\Delta^2(\Psi) - 2qp''\Delta(\Psi)\Delta(x+\Psi) \\
& + \frac{1}{2}qp''\Delta^2(x+\Psi) - 2qp\Delta''(x+\Psi)\Delta(\Psi) + qp\Delta''(x+\Psi)\Delta(x+\Psi) \\
& + qp\Delta'(x+\Psi)^2 + 2p'\Delta'(x+\Psi)\Delta(x+\Psi) + \frac{1}{2}p''\Delta^2(x+\Psi) \\
& + p\Delta''(x+\Psi)\Delta(x+\Psi) + p\Delta'(x+\Psi)^2 + \frac{1}{2}p''\Delta^2(\Psi)\Big)\, d\Psi \\
- \int_0^1 & \; r\left(\frac{q+1}{2}\right)^2 [\Delta(\Psi) - \bar{\Delta}][\; (p\Delta(\Psi) - p'\Delta(x+\Psi) - p\Delta'(x+\Psi))\; d\Psi].
\end{aligned} \tag{2.7}$$

The second integral arises as a consequence of the order ϵ terms in the density function, $\varphi(\Psi)$. Let us define

$$h(x) := \int_0^1 \Delta(\Psi)\Delta(\Psi + x)\; d\Psi$$

and observe the following:

$$\begin{aligned}
\int_0^1 \Delta(\Psi)\; d\Psi &= \int_0^1 \Delta(x+\Psi)\; d\Psi \\
\int_0^1 \Delta''(\Psi)\Delta(\Psi)\; d\Psi &= -\int_0^1 \Delta'(\Psi)^2\; d\Psi.
\end{aligned}$$

With these definitions, observations, and the fact that $\Delta(\Psi)$ is periodic, we can simplify (2.7) to

$$\begin{aligned}
0 \; = & -4qp'h'(x) + (1+q)p''h(0) - 2qp''h(x) - \\
& 2qph''(x) + r\frac{(q+1)^2}{4}[h'(x)p + (h(x) - h(0))p']
\end{aligned} \tag{2.8}$$

If $G(x) = 1 - \dfrac{2q}{(1+q)}\dfrac{h(x)}{h(0)}$ and
$H(x) = \dfrac{(1+q)}{4}\left(1 - \dfrac{h(x)}{h(0)}\right)$, then (2.8) is equivalent to

$$[p(x)G(x)]'' - r[p(x)H(x)]' = 0. \tag{2.9}$$

This can be integrated to yield a complex expression for the density function for the phase-differences. However, it is much easier to first consider the low rate approximation where

$r = 0$. Using boundary conditions $p(0) = p(1)$ we can solve for constants C_1 and C_2 in the solution to the second order differential equation in (2.9):

$$p(x)G(x) = C_1 x + C_2$$
$$C_1 = 0 \ , \ C_2 = \frac{1}{\int_0^1 \frac{1}{G(x)}\, dx}$$

where the condition on C_1 comes from the periodicity of $p(x)$ and the condition on C_2 from the normalization of $p(x)$. Thus

$$p(x) = \frac{C_2}{1 - c\frac{h(x)}{h(0)}},$$

where we have substituted $c = 2q/(1+q)$, the value of the input correlation. Thus, for low rate Poisson inputs with a small PRC we obtain exactly the same equation for the density of phase differences as was derived by Nakao et al [66] for the white noise case. We summarize the result as follows. For two identical oscillators with input correlation, c and slow Poisson impulses, the density of the phase differences is given by:

$$p(x) = \frac{N}{1 - c\frac{h(x)}{h(0)}} \tag{2.10}$$

where $h(x)$ is the autocorrelation of the PRC, where N is the normalization term C_2. As $c \to 1$, $p(x) \to \delta(x)$, the Dirac delta function. Thus perfectly correlated noisy oscillators will synchronize with zero phase lag. If $c = 0$, then $p(x) = 1$ is uniform.

The full equation (2.9) with $r \neq 0$ can be solved exactly but little intuition can be gained. In Fig. 2.2.2, we show the numerical solution to (2.9) for two different values of q and for various values of the rate, r. At the high value, $q = 0.8$ corresponding to 80% shared input ($c = 8/9$), the effects of the Poisson rate on the shape of the stationary density $p(x)$ are minimal. At lower correlation, e.g. 20% shared input ($c = 1/3$), the rate has a stronger effect although it is still quite small. Heterogeneity in the actual frequencies of the two oscillators will contribute a term of the form $(-p(x)\mu)'$ to the left hand side of (2.9), where μ is the difference in the frequencies of the two oscillators. Thus drift will shift the peak of $p(x)$, but will not significantly change the width of the peak. Thus, we will ignore heterogeneity from now on.

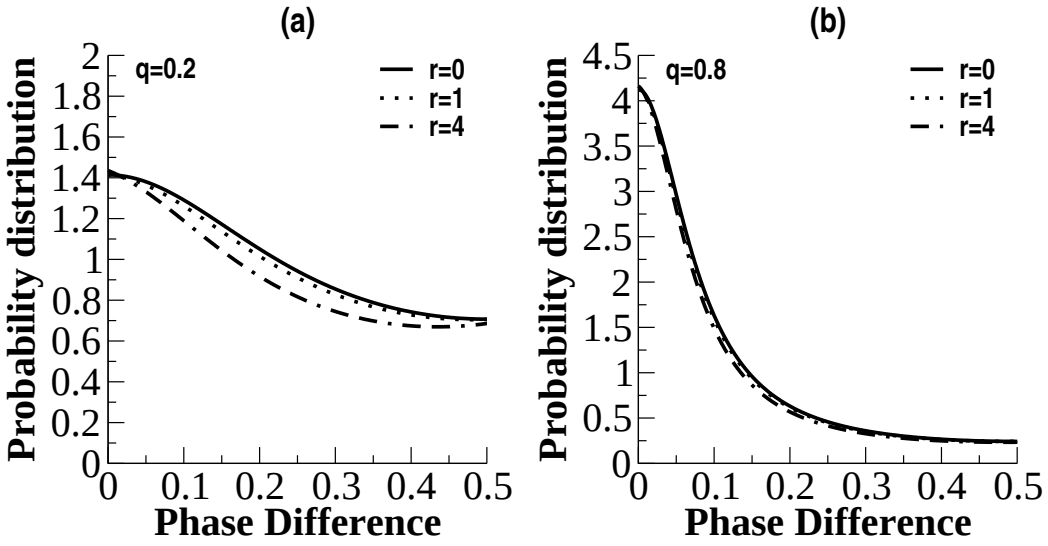

Figure 1: Steady state density $p(x)$ for $q = 0.2$ and $q = 0.8$ with different values of the Poisson rate, r.

In the remainder of the paper, we explore how the shape of the PRC affects the degree of synchronization with partially correlated inputs using the small r approximation (2.10) . Since equation (2.10) is the same as derived in Nakao et al [66], what we conclude about shape and synchrony for Poisson inputs will also hold for white noise.

In order to quantify difference in the shapes of the density, $p(x)$, we need to introduce some measure of the degree of synchrony. We will analyze several different measures. The simplest is:

$$z_1 = \int_0^1 \cos(2\pi x) p(x)\, dx. \tag{2.11}$$

If $p(x)$ is uniform, then z_1=0 and if $p(x)$ is a delta function, z_1=1. The *circular variance* or *vector strength* [5] of a distribution on the circle is defined as

$$\mathrm{Var}(\theta) = 1 - R/n$$

where

$$R^2 = \left(\sum_{j=1}^{n} \cos 2\pi\theta_j \right)^2 + \left(\sum_{j=1}^{n} \sin 2\pi\theta_j \right)^2 .$$

Circular variance characterizes phase locking between oscillators. Since $p(x)$ is symmetric for identical oscillators, the sine average of the phases vanishes, and our order parameter is exactly R/n. Thus, the circular variance, $1 - z_1$, is a good measure of the tightness of the distribution on the circle. For sharp distributions, higher order circular moments may be a better measure, e.g.

$$z_j = \int_0^1 \cos(2\pi j x) p(x)\ dx$$

since z_1 measures how close $p(x)$ is to a pure cosine curve. We use the first n of order parameters, and take the limit as $n \to \infty$, we obtain a general order parameter, $p(0) - 1$ (see section 2.7). A common measure that is used in neuroscience is the cross correlation. However, for this to make sense, we need to map the phase model onto a "spike train." Pfeuty et al [70] consider a simple example $S_j(t)$, defined to be $1/\delta$ if $\theta_j(t)$ is within δ of $\theta = 0$ and $S_j(t) = 0$ otherwise. They show that the cross correlation of two such spike trains is just $p(x)$, that is:

$$\frac{\langle S_1(t_1) S_2(t_2) \rangle}{\langle S_1(t) \rangle \langle S_2(t) \rangle} = p(t_2 - t_1).$$

Thus, a measure of the degree of synchrony is the peak, $p(0)$ which is related to our generalized order parameter. Like that parameter, there is no simple way to normalize this cross-correlation.

2.3 EXAMPLES

2.3.1 Comparison with simulations

We first illustrate how well the theory works by comparing Monte-Carlo simulations with the equation (2.10) and varying the amplitude of the PRC and the rate of the Poisson process. Fig. 2.3.1 shows an example Monte-Carlo simulation of equations (2.2-2.3) for different Poisson rates and for different PRC amplitudes using a sinusoidal PRC. We iterate 10^6 times and bin the resulting data into 100 bins between -0.5 and 0.5. Over a range of two orders of magnitude in the Poisson rates, there is no difference in the shape of the density function. Similarly, for small amplitudes, there are no differences in the density either.

However, if the amplitude becomes large enough, then the approximation of uniformity for the phase of individual oscillators breaks down and equation (2.10) becomes inaccurate. For example, Fig. 2.3.1(d) shows the density of the oscillator phase in equation (2.2) as the amplitude of the PRC increases. Finally, with a modest amplitude, equation (2.10) provides a precise approximation of the Monte-Carlo histogram as shown in Fig. 2.3.1(c).

2.3.2 Shape matters

We use the terms 'Type I' and 'Type II' to refer to the PRC's of Class I and Class II neurons respectively and use, $1 - \cos(\theta)$ and $\sin(\theta)$ as their respective idealizations. Theoretical predictions for the probability density functions of phase differences for classical type I and type II PRCs can be obtained from equation (2.10). For two sample values of q, we show that type II oscillators have a narrower distribution of phase differences around zero, compared to type I as can be seen in Fig. 2.3.2. Note that both these oscillator types will synchronize at identical rates if $q = 1$ since their Lyapunov exponents are the same [93] . Using equation (2.11) we calculated the circular variance of the distribution obtained from equation (2.10). Since physical systems like postsynaptic neurons have to accommodate jitter around a zero difference in the presynaptic spike times, we calculated the probability that the phase difference lies within a 0.2T interval around zero. i.e. $\text{Prob}(\delta \in [-0.1, 0.1])$. In Fig. 2.3.2(b) and all subsequent plots, $\text{Prob}(\delta \in [-0.1, 0.1])$ is plotted after subtracting its value at $q = 0$, hence the plot purely reflects the contribution of non-zero q. In Fig. 2.3.2(a), it can be seen that the circular variance of the phase differences for type II is lower (higher values of the order parameter z_1) than that for type I oscillators for all possible values of q. In Fig. 2.3.2(b), it can be seen that there is a higher probability for type II oscillators to stay closer in phase than type I. We note that choice of the length of the interval is arbitrary and the relationship between the curves is conserved at other choices of interval lengths. Taken together, these three results show that for any given input correlation $c < 1$, type II oscillators have a higher probability of undergoing stochastic synchronization compared to type I for non-zero q. This observation supports the hypothesis that the shape of the PRC can determine the degree to which uncoupled oscillators can synchronize under the influence

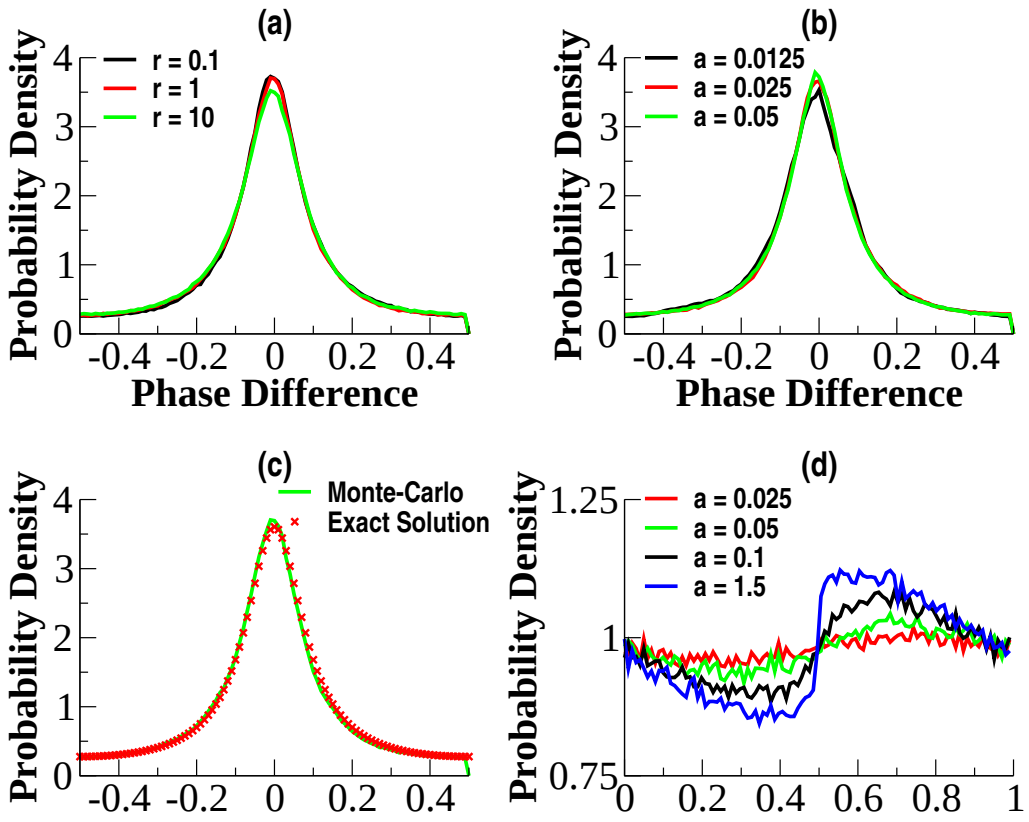

Figure 2: Monte-Carlo simulations for $\Delta(x) = a \sin 2\pi x$ with $q = 0.75$ and Poisson rate r. 10^6 iterations are run and binned in 100 bins on the interval $[-.5, .5)$. (a) Independence of the rate for $r = 0.1, 1, 10$ at $a = 0.025$ (b) Independence of the amplitude for small amplitude s, $a = 0.0125, 0.025, 0.05$. at $r = 1$ (c) Comparison of the $r = 1, a = 0.025$ case for $q = 0.75$ with the density from equation (2.10). (d) Larger amplitudes result in more non-uniformity in the distribution of individual oscillator phases at rate $r = 1$.

of noise.

For small values of input correlation, c, we can get an approximation for the order parameter as well as the peak of the density function. For c small,

$$p(x) = \frac{N}{1 - ch(x)/h(0)} \approx N(1 + ch(x)/h(0))$$

from which we find that

$$N \approx 1 - c \int_0^1 h(x)/h(0)\ dx := 1 - c\,\langle h \rangle / h(0)$$

so that

$$p(0) - 1 \approx c(1 - \langle h \rangle / h(0)).$$

Thus, the peak of the probability distribution function and the generalized order parameter are maximized when the average value of $h(x)$ is zero. Recalling the definition of $h(x)$, we obtain the concise formula for small correlations:

$$p(0) - 1 \approx c \left[1 - \frac{\langle \Delta \rangle^2}{\langle \Delta^2 \rangle} \right]. \tag{2.12}$$

Holding the L_2 *norm* of Δ constant $\sqrt{\langle \Delta^2 \rangle}$, we see that DC component of Δ is what hurts the ability to synchronize at low input correlation. Type II oscillators have a lower DC component and thus synchronize more readily.

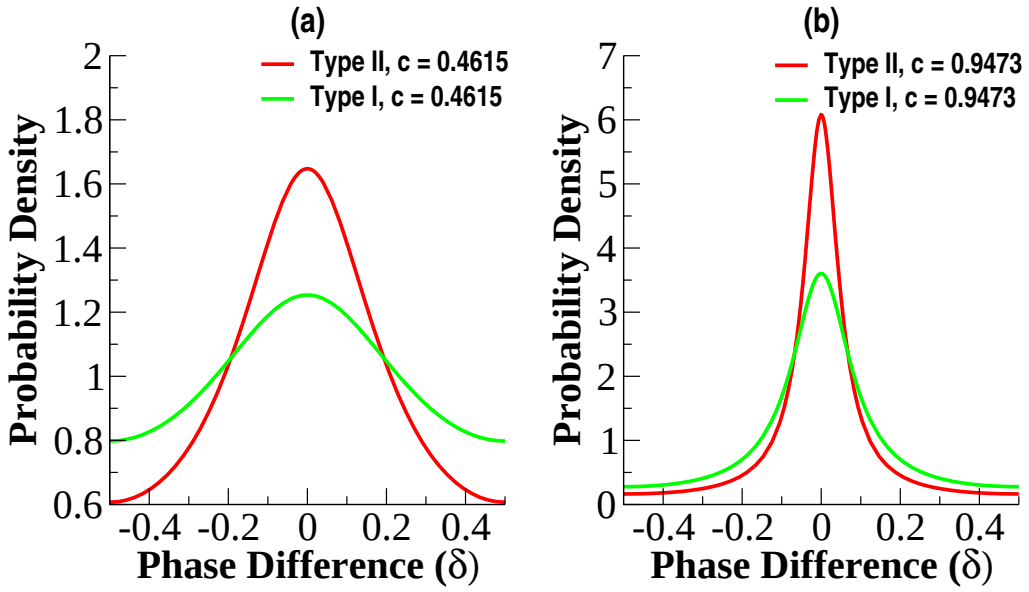

Figure 3: Simulation results showing distribution of phase differences for type I and type II PRCs, at two different input correlations ($q = 0.3$ and $q = 0.9$). Probability is plotted along the ordinate and the phase differences on the abscissa.

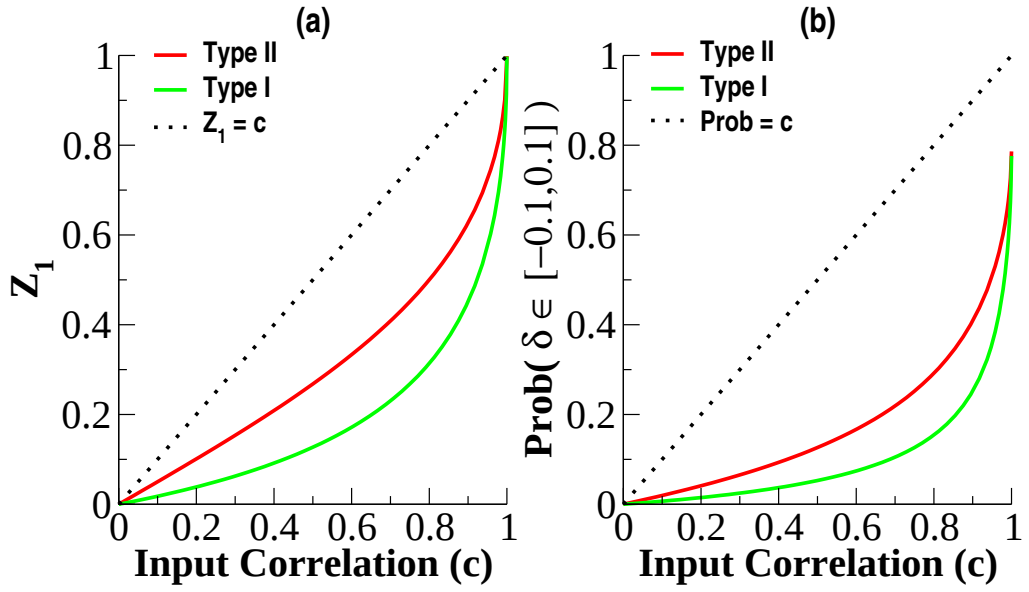

Figure 4: Comparison of the order parameter between type I and type II PRCs.

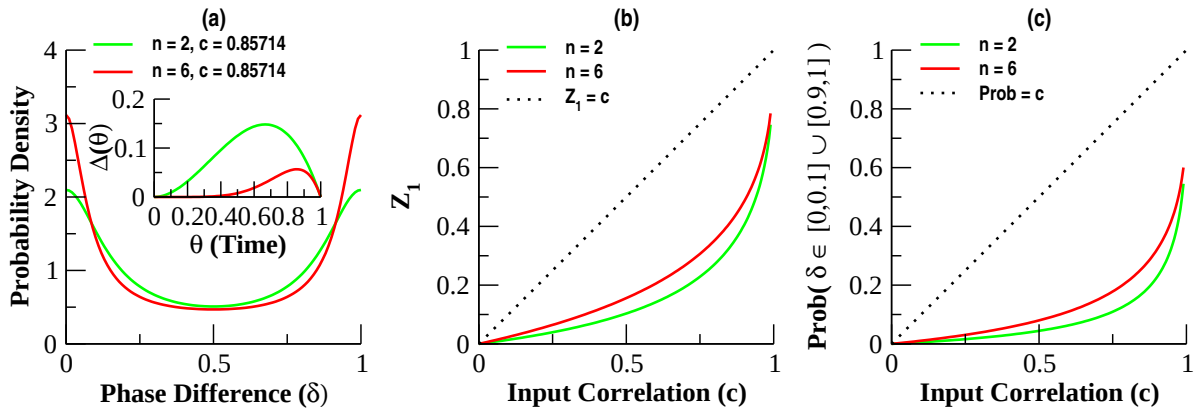

Figure 5: Simulations showing the effect of firing rate on stochastic synchronization. PRCs from Gutkin et al 2005 [43] were fit using $x^n(1-x)^m$ where the values of $n = 2, m = 1$ and $n = 6, m = 1$ were used to fit the high and low frequency firing respectively. Inset in (a) shows PRC's for both frequencies for $q = 0.75$.

2.3.3 Dependence on firing rate

We also investigated the influence of firing rate on stochastic synchronization. PRCs for a model neuron obtained in low and high firing frequency regimes [43] were fit using a polynomial function $x^n(x-1)^m$. Both PRCs were type I, i.e. the membership of the PRC remained type I in both the frequency regimes. Using these fits, we calculated the probability density of the phase differences and $1-$ circular variance. The results are plotted in Fig. 2.3.3. It can be seen that for higher firing rate (corresponding to n=2,m=1) there is a broader distribution of phase difference around zero and also a higher circular variance (lower values of the order parameter z_1). These results suggest that increase in firing frequency decreases the probability of synchronization due to stochastic input for a type I PRC.

Firing rate dependence of stochastic synchronization was investigated in another model neuron, specifically the Morris Lecar (ML) system. The parameters for the model can be tuned such that the model displays either a type I or type II PRC. In both these regimes the PRC has a tendency to become more negative with an increase in the input current.

For a ML system with a type I PRC under moderate current conditions, this translates to a conversion from a classic type I to a type II PRC. A type II ML system on the other hand continues to experience an increase in its negative part with an increase in input current. Fig.2.3.3 shows a ML system with a type I PRC. It can be seen that there is narrowing of the distribution of phase differences accompanied by lower circular variance for the system firing at a higher frequency with a type II PRC. A similar transition can be observed for a ML system with parameters set to a type II PRC regime (Fig. 2.3.3), but the magnitude of change is much less, since the system has a type II PRC at the outset as can be seen in Fig. 2.3.3 and Fig. 2.3.3.

The leaky integrate and fire (LIF) model is used widely as a first approximation to continuous and realistic neuronal models, thus, it is important to understand the behavior of LIF neurons in a stochastic synchronization paradigm. In order to derive the order parameter for two LIF neurons we first obtained the PRC using the adjoint method. Briefly, if

$$\frac{dX}{dt} = F(X)$$

is a differential system in R^n and $X_0(t)$ is its T-periodic limit cycle solution. Then $x = X_0(t)$ is a point on the limit cycle at time(phase) t. The PRC is given by the function $Z(\phi)$ where,

$$Z(\phi) = \nabla_X(\Theta(X_0(\phi)))$$

and $\Theta(x)$ is the phase function that relates a point on the limit cycle to its phase ϕ and is defined as

$$\Theta(X_0(\phi))) = \phi. \tag{2.13}$$

Differentiating (2.13) with respect to ϕ gives a relation between the PRC and $F(X)$

$$Z(\phi)^T \frac{dX_0}{d\phi} = 1.$$

We derived the PRC for the LIF using the above formulation. Since, we are in one dimension, this implies

$$Z(\phi) = \frac{1}{\frac{dX_0}{d\phi}}.$$

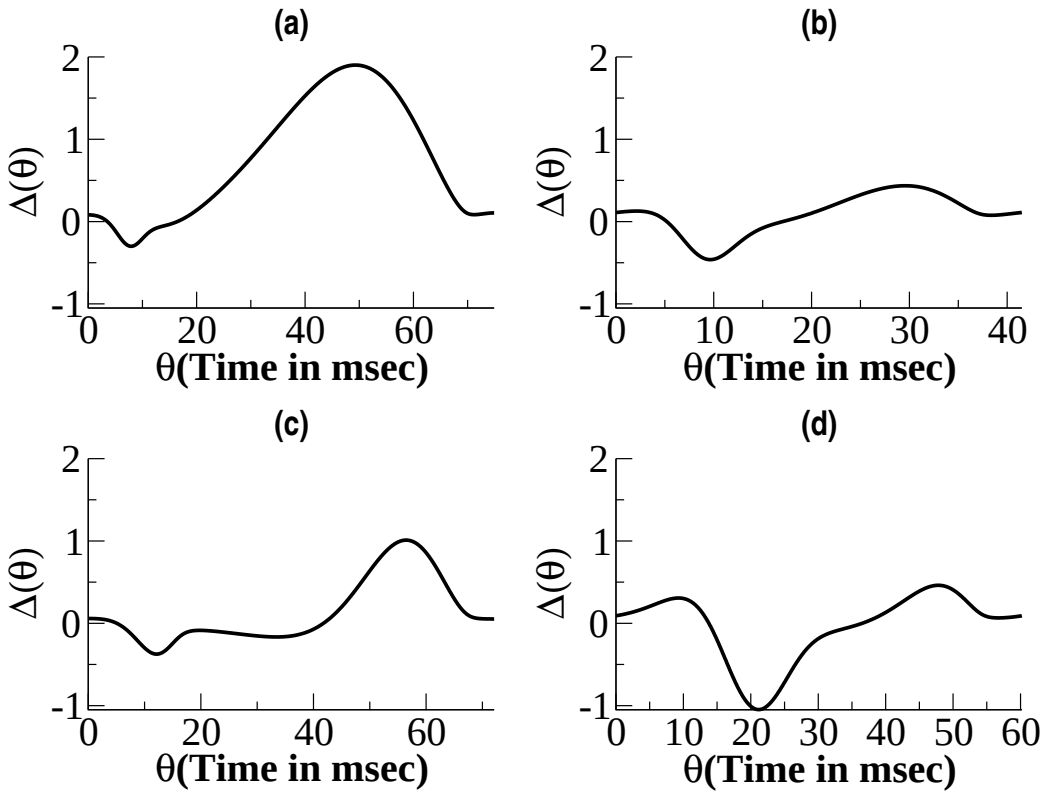

Figure 6: Transformation of the PRC for the ML system in different frequency regimes.(a) ML system in type I regime with an injected current of 50 μA (threshold around 40 μA). The PRC is almost completely type I (b) PRC of ML system in A after the injected current is increased to 100 μA. The PRC is transformed to the type II regime (c) ML system in type II regime with an injected current of 120μA (threshold around 100 μA. The PRC is type II (d) Transformation of PRC in C upon increasing injected current to 220 μA

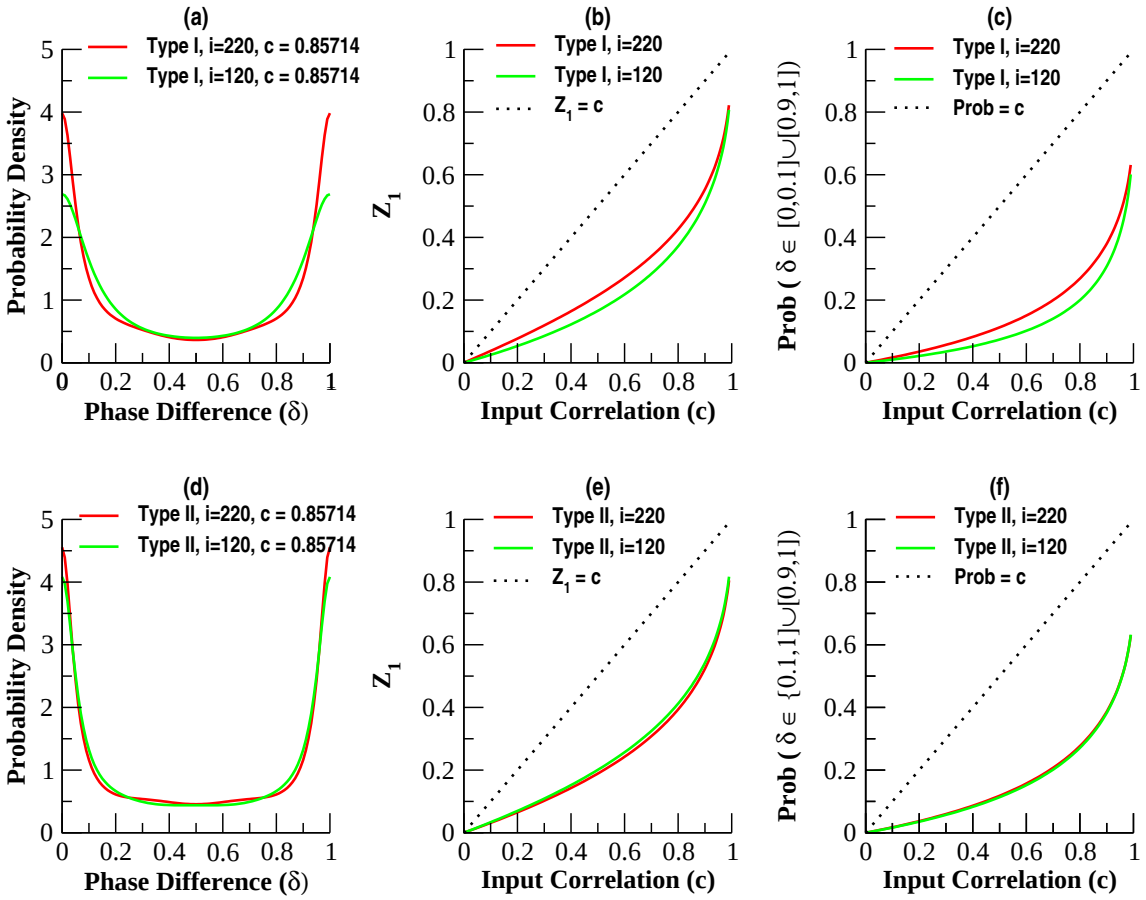

Figure 7: Simulations showing the effect of firing frequency on stochastic synchrony in type I and type II Morris-Lecar system. The different input currents were I=50,100 for type I and I=120,220 for type II,$q = 0.75$ for (a) and (d)

The LIF in its most general form is given as.

$$\frac{dV}{dt} = -V + I. \tag{2.14}$$

Solving (2.14) we get

$$V(t) = I - Ie^{-t}. \tag{2.15}$$

The PRC is obtained by taking the reciprocal of the derivative of (2.15) with respect to t. Therefore,

$$Z(\phi) = \frac{e^{\phi}}{I}.$$

We calculated the autocorrelation function $h(x)$ of the PRC as follows

$$\begin{aligned} h(x) &= \int_0^{P-x} e^y e^{x+y} dy + \int_{P-x}^{P} e^y e^{x+y-P} dy \\ &= \tfrac{1}{2}\left[e^{P-x}(e^P - 1) + e^x(e^P - 1)\right]. \end{aligned}$$

For calculating the order parameter for different periods we used the following simplifications.

$$H(x) = \frac{h(x)}{h(0)} = \frac{e^{P-x} + e^x}{e^P + 1}. \tag{2.16}$$

In order to parametrize the phase x we replace it with sP where $s \in [0, 1]$ and we can write (2.16) as

$$H(s, P) = \frac{e^{-Ps} + e^{P(s-1)}}{1 + e^{-P}}. \tag{2.17}$$

Using this we calculated the order parameter for different periods in Fig. 2.3.3. It can be observed that the order parameter is a non-monotonic function of the period of oscillation. We plot the order parameter as a function of period for $q = 0.75$ in Fig. 2.3.3. The position of the maxima of the order parameter curves depend on the period of oscillation. We show the order parameter obtained for a range of values for q and P in Fig. 2.3.3.

The Wang-Buzsaki model is a commonly used model for cortical interneurons [101]. It has a very wide range of frequencies and thus we investigated how this model is able to synchronize under a stochastic synchronization paradigm at different frequencies. The adjoint was numerically calculated at different frequencies and the slope of the generalized order parameter with respect to input correlation was calculated as given in equation (2.12)

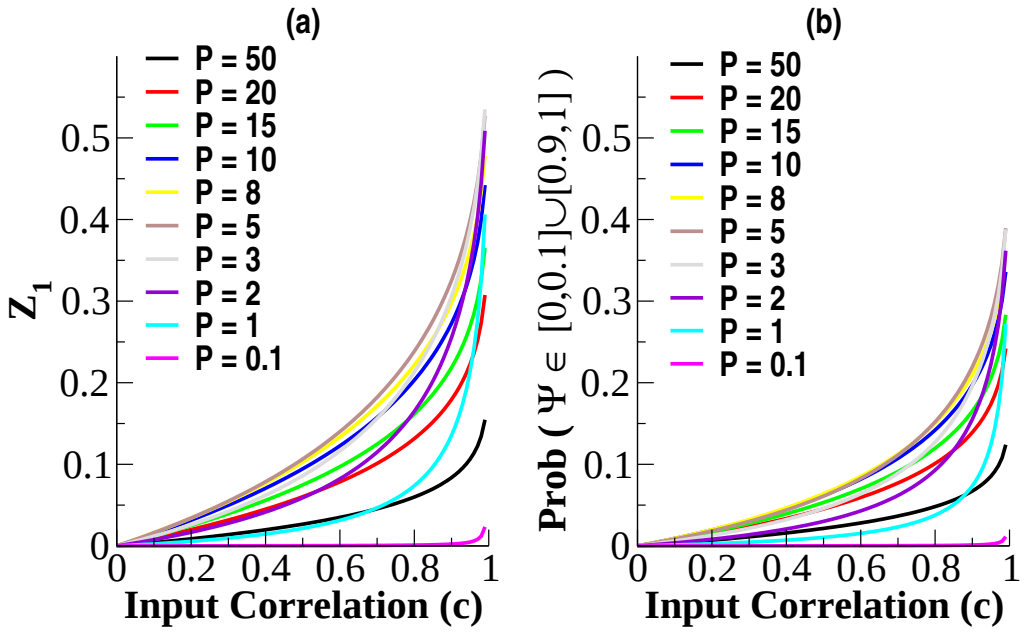

Figure 8: Comparison of the order parameter obtained using an LIF neurons at different firing frequencies. Numbers indicate the time period between two successive spikes,$q \in [0, 1)$.

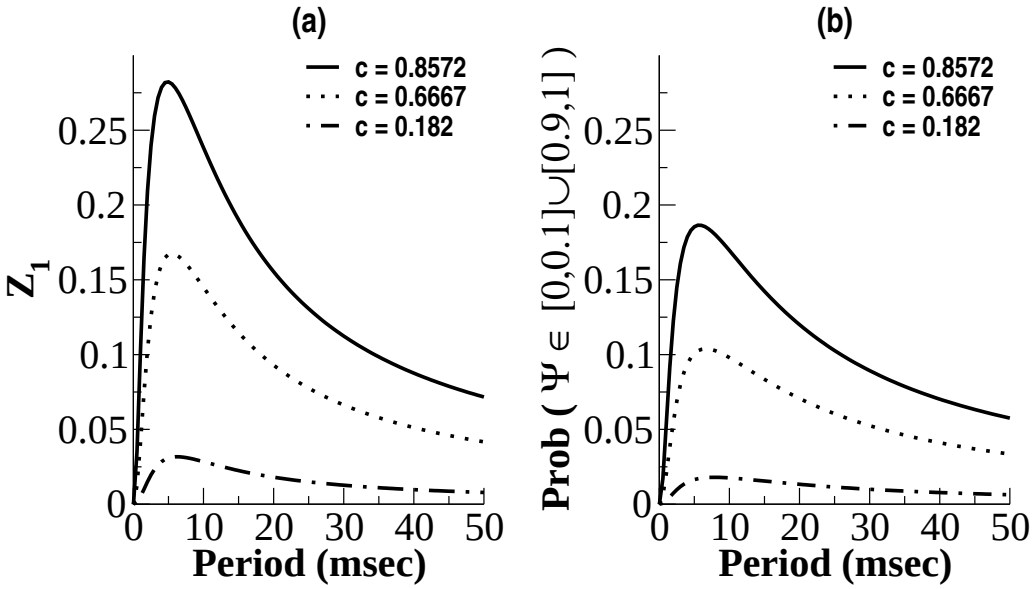

Figure 9: Comparison of the order parameter obtained using LIF neurons at different periods at $q = 0.75$,$c = 0.85714$

and plotted in Fig. 2.3.3. It can be seen that the rate of change for the generalized order parameter has a sublinear relationship with respect to input correlation c, through almost the entire range of the neuron's firing frequency except possibly at the neuron's highest firing frequency where it reaches a value of 1, hence becoming linear. Additionally, this rate of change of the generalized order parameter with respect to the input correlation c, has a non-monotonic relationship with respect to the firing frequency of the neuron wherein, in the lower frequency range it decreases from a value 0.5, close to 0 Hz to about 0.29 at around 33 Hz and then increases up to a value of 0.75 at around 400 Hz followed by a rapid increase to a value of 1 at the neuron's highest firing frequency around 500 Hz.

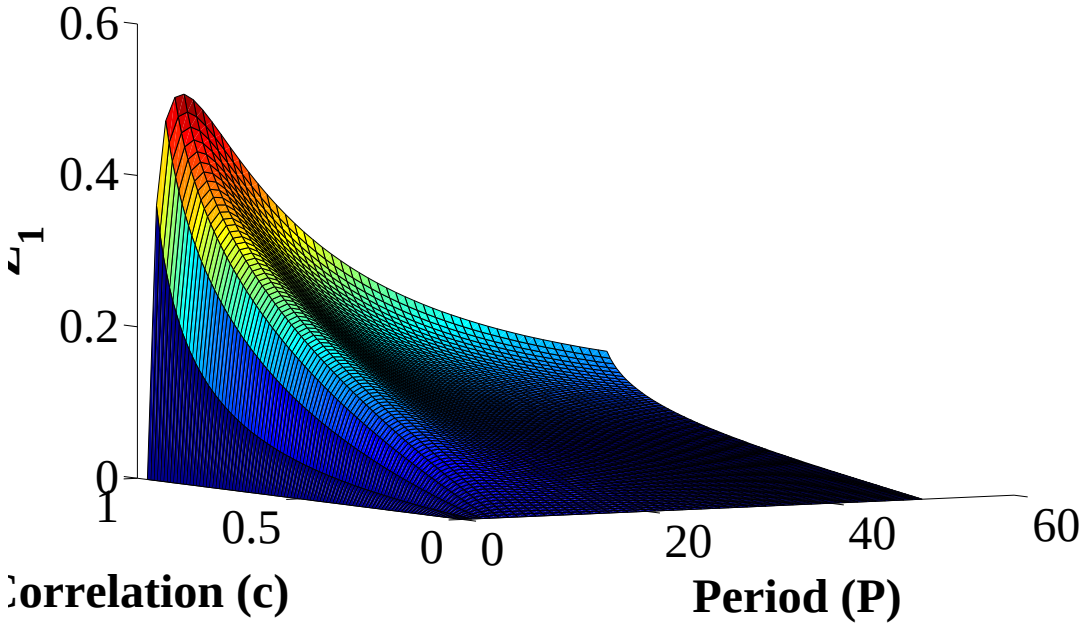

Figure 10: Order parameter obtained from LIF neurons over a range of $q \in [0, 1)$ and $P \in (0, 50]$

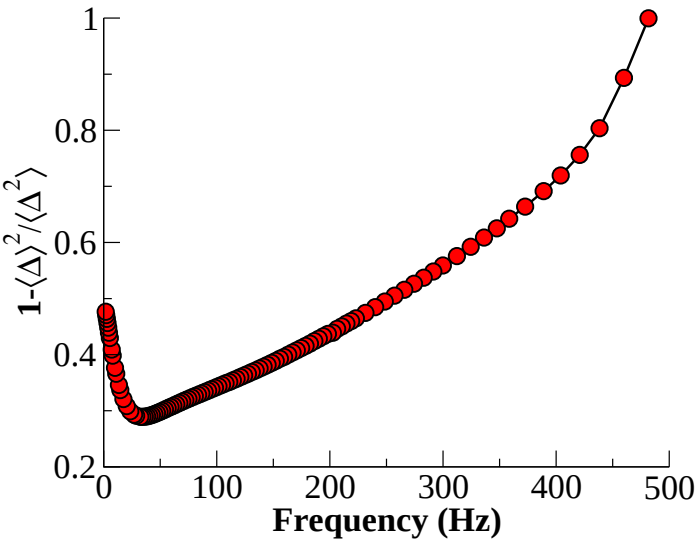

Figure 11: Slope for the generalized order parameter and input correlation dependence from Wang-Buzsaki model over a range of firing frequencies

2.4 DISCUSSION

In this work, we analyzed a system of identical, uncoupled limit-cycle oscillators receiving weak, partially correlated, Poisson distributed inputs. We derived an expression (2.9) for the probability density function of the phase difference between the two oscillators. Numerical simulations of (2.9) suggest a relative independence of the phase distribution with respect to the input rates at moderate to high input correlation values (Fig. 2.2.2) and weak inputs (Fig. 2.3.1). Thus we analyzed (2.9) under the assumption of low rates which makes it possible to gain an intuitive understanding of the mechanism of PRC-shape dependent stochastic synchrony. Our results suggest that the shape of the PRC is crucial in controlling the magnitude of stochastic synchrony realized by the system.

By adopting circular variance as a measure of synchrony we show that Type II PRCs tend to show higher synchrony than Type I PRCs at all values of input correlation (Fig. 2.3.2). This result is also reflected identically in another measure of synchrony where we simply integrate the probability density between arbitrary upper and lower limits around

zero. These results taken together suggest that the phase differences for oscillators with Type II PRCs are more densely clustered around zero compared to systems with Type I PRCs which show longer tails. In other words, systems with Type II PRCs spend more time close to each other than those with Type I PRCs. We also show that the generalized order parameter, which is simply the sum of the correlations between the phase distribution function and all modes of cosine, is linear in the input correlation, for weak correlations.

In real neurons the shape of the PRC can be modulated by the firing frequency [43]. This modulation is mediated by slow adaptation processes, mainly slow potassium currents which increase with an increase in firing frequency. But this increase in the slow potassium current also decreases the fractional contribution of the transient potassium currents at the start of the inter spike interval (ISI) which causes an otherwise skewed PRC at moderate firing frequencies to become less skewed at higher frequencies. Our investigation suggests that synchronization is affected by firing frequency and decreases at higher frequencies (Fig. 2.3.3). That this difference in synchronization is observed without the change in the membership of the PRC (Type I at both frequencies) only solidifies the role of subtle differences in the shape of PRC, in this case the degree of skewness, in dictating the system's propensity for undergoing stochastic synchronization.

In the light of the above results, we investigated a system whose PRC undergoes substantial modulation in shape and changes membership at higher frequencies. Our results from simulations using the Morris-Lecar model show that stochastic synchrony increases with firing frequency as the PRC changes from a Type I to Type II. In contrast, when the system starts out in a Type II regime, the change in the circular variance due to increase in firing frequency is minimal. A recent study, set in a similar setting has shown that the output correlation of spike counts between LIF neurons increases with firing frequency [15]. Our results show a non-monotonic relationship between circular variance of the phase differences and firing frequency. The circular variance of the phase difference does decrease with increase in firing frequency but only up to a point beyond which it increases with frequency. We also note that the LIF has a Type I PRC at all firing frequencies. At this point the interrelationship between these different measures is unclear. A similar firing rate dependence was also observed for the Wang-Buzsaki model. The relationship between the slope of

the generalized order parameter with respect to input correlation (2.12) and the firing rate was non-monotonic Fig. 2.3.3, hence the relative increase in the generalized order parameter with respect to input correlation will be determined by the frequency of firing, similar to the observations in LIF. Such a firing rate dependent spike time cross-correlation has been reported in a recent study [52](Figure 8).

Our results suggest a strong effect of the shape of PRC on the synchronization properties of the cell. The shape of the PRC is determined by the variety of ion-channels that define the dynamical behavior of a neuron. The relative contribution to membrane voltage of these ion-channels depends on the firing rate of the neuron. We have described a mechanism by which these interactions might occur and finally be reflected in the spike time correlation of general oscillator systems.

2.5 INPUT CORRELATION

Consider a Poisson process with rate r For each spike let c be the probability that an oscillator receives that particular spike. The effective rate of the Poisson process for the neuron is just cr. Consider a pair of neurons. The probability that they both receive the given spike is c^2 and the probability that one receives a spike and the other does not is $c(1-c)$. Thus, c^2 is the fraction of shared inputs and c is the correlation of the inputs. $(1-c)^2$ is the probability that neither receives an input. For our problem, as the oscillators are identical, if neither receives input, then their phase difference remains the same until the next input comes in. Thus, the only cases in which an event occurs that changes the phases are those in which at least one oscillator receives an input. The fraction of relevant events (those in which at least one oscillator gets an input) with shared inputs is $c^2/(1-(1-c)^2) = c/(2-c)$. Recalling that q is the fraction of shared inputs, we see that $q = c/(2-c)$ or, $c = 2q/(1+q)$. Thus, the quantity, $2q/(1+q)$ is the input correlation.

2.6 INVARIANT DENSITY

The invariant density, $\varphi(x)$ satisfies:

$$\begin{aligned}\varphi(x) &= \frac{1-q}{2}\int_0^1 Q(x-y)\varphi(y)\ dy \\ &\quad + \frac{1+q}{2}\int_0^1 Q(x-y-\epsilon\Delta(y))\varphi(y)\ dy.\end{aligned}$$

Here $Q(x)$ is the inter-spike interval or the waiting time density for a Poisson distribution with rate r modulo 1,

$$Q(x) = \frac{re^{-rx}}{1-e^{-r}}.$$

For $\epsilon = 0$, $\varphi(x) = 1$, so we expand in terms of ϵ to get the next order: $\varphi(x) = 1+\epsilon\varphi_1(x)+\ldots$. The next order equation is

$$\varphi_1(x) = \int_0^1 Q(x-y)\varphi_1(y) - \frac{1+q}{2}\int_0^1 Q(x-y)\Delta'(y)\ dy$$

along with the condition that the mean value of $\varphi_1(x)$ is zero (since the integral $\varphi(x)$ must be one for normalization). For general $Q(x)$ we can solve for $\varphi_1(x)$ by using a Fourier expansion. Specifically, write

$$\begin{aligned}\varphi_1(x) &= \sum_n b_n e^{2\pi inx} \\ Q(x) &= \sum_n q_n e^{2\pi inx} \\ \Delta(x) &= \sum_n d_n e^{2\pi inx}.\end{aligned}$$

We must then have

$$b_n = -\frac{1+q}{2}\frac{2\pi i n q_n}{1-q_n}d_n.$$

For a Poisson process with rate r

$$q_n = \frac{r}{r+2\pi in}$$

so that

$$b_n = -r\frac{1+q}{2}d_n$$

as long as $n \neq 0$. (For $n = 0$, $b_0 = 0$ since the next order terms must have zero mean. Thus,

$$\varphi_1(x) = -r\frac{1+q}{2}(\Delta(x) - \int_0^1 \Delta(x)\ dx).$$

2.7 ORDER PARAMETERS

Consider the order parameters,

$$z_j = \int_0^1 p(y) \cos 2\pi j y \; dy, \quad j \geq 1.$$

If $p(x)$ is uniform, then each of these vanishes and if $p(x)$ is a delta function, then $z_j = 1$. Consider the sum of these order parameters as a measure of the synchrony in all modes:

$$Z = \lim_{N \to \infty} \sum_{j=0}^{N} z_j - 1.$$

We have included z_0 in the sum and subtracted 1 from the total to compensate. Now, we formally rearrange the sum

$$Z = \int_0^1 p(x) \left[\lim_{N \to \infty} \sum_{j=1}^{N} \cos 2\pi j x \right] \; dx - 1.$$

The sum in the brackets forms a "delta-sequence" (that is, in the limit, this sum goes to a Dirac delta function) (c.f. [51]). Thus, $Z = p(0) - 1$, exactly as derived above. For this reason, we treat $p(0) - 1$, a generalized order parameter, as a measure of the local synchrony and correlation.

2.8 MODEL EQUATIONS

2.8.1 Morris Lecar Model

$$C_m\frac{dV}{dt} = g_L(V_L - V) + g_K w(V_K - V) + g_{Ca}m_\infty(v_{Ca} - V) + I\frac{dw}{dt} = \lambda_w(w_\infty - w)$$

$$m_\infty(V) = 0.5(1 + \tanh((V - V_1)/V_2))$$

$$w_\infty(V) = 0.5(1 + \tanh((V - V_3)/V_4))$$

$$\lambda_w(\phi, V) = \phi\cosh(0.5(V - V_3)/(V_4))$$

For a Type II model, $V_K = -84$, $V_L = -60$, $V_Ca = 120$, $g_K = 8$, $g_L = 2$, $g_{Ca} = 4$, $C_m = 20$, $V_1 = -1.2$, $V_2 = 18$, $V_3 = 2$, $V_4 = 30$, $\phi = 0.04$, for a Type I model we changed the following parameters $V_3 = 12$, $V_4 = 17$, $\phi = 0.0667$.

2.8.2 Wang Buzsaki Model

$$\begin{aligned} C_m\frac{dV}{dt} &= g_L(V_L - V) + g_{Na}m_\infty^3 h(V_{Na} - V) + g_K(n^4)(V_K - V) + I \\ m_\infty &= a_m/(a_m + b_m) \\ a_m(V) &= -0.1(V + 35)/(\exp(-0.1(V + 35)) - 1) \\ b_m(V) &= 4\exp(-(V + 60)/18) \\ \frac{dh}{dt} &= \phi(a_h(V)(1 - h) - b_h(V)h) \\ a_h(V) &= 0.07\exp(-(V + 58)/20) \\ b_h(V) &= 1/(\exp(-0.1(V + 28)) + 1) \\ \frac{dn}{dt} &= \phi(a_n(V)(1 - n) - b_n(V)n) \\ a_n(V) &= -0.01(V + 34)/(\exp(-0.1(V + 34)) - 1) \\ b_n(V) &= 0.125\exp(-(V + 44)/80) \end{aligned}$$

$C_m = 1$, $g_L = 0.1$, $V_L = -65$, $g_{Na} = 35$, $V_{Na} = 55$, $\phi = 5$, $g_K = 9$, $V_K = -90$

3.0 AMPLIFICATION OF STOCHASTIC SYNCHRONIZATION IN RECURRENT NETWORKS

The topics treated in this chapter can be somewhat obscure. For humanitarian considerations, the chapter will be subdivided [82]

3.1 INTRODUCTION

The topic treated here, given its complexity, merits an additional subdivision.

Synchronization of neural activity has been suggested to facilitate coding [20, 86, 87] and propagation of activity [79, 77, 94]. Synchronous stimulus-induced oscillatory activity has long been known to occur in the olfactory system of mammals [2, 3, 10, 83, 18]. Synchronous, rhythmic activity has been proposed to play a role in odor discrimination tasks [50]. In insects, disruption of synchronous oscillations can impair discrimination of chemically similar odorants [89]. In mice, enhancement of synchronous oscillations in the olfactory bulb using genetic modifications improves performance in fine discrimination tasks [68]. In the mammalian olfactory system, mitral cell synchrony contributes to the generation of the gamma oscillations in the local field potential; for example, in the cat olfactory system, increases in the synchrony between mitral cells are accompanied by a concomitant increase in the power of the gamma band in the local field potential [29]. Mitral cells have been shown to undergo synchronization during odor-evoked responses [49] or during olfactory nerve stimulation [82]. Although, previous experimental and modeling studies have highlighted the role of granule cells [55] and lateral inhibition [7] in the production of gamma oscillations in the olfactory bulb, the exact mechanism by which such mitral cell synchronization occurs

in the mitral-granule cell network connected by reciprocal recurrent and lateral connections remains largely unknown.

A possible mechanism of synchronization of mitral cells in the olfactory bulb is suggested by recent experimental evidence. In paired recordings from mitral cells, activation of a mitral cell elicits fast unitary inhibitory post-synaptic potentials (IPSC's) in a second mitral cell [98, 33, 82]. These IPSC's are due to the synaptic activation of the shared granule cells via the mitral-granule cell dendrodendritic synapses. Although the individual IPSC's are fast , they arrive randomly (asynchronously), i.e. the output of the granule cells is not time locked to the stimulus. The temporally prolonged barrage of these unitary IPSC's produced in response to the spiking in the first mitral cell results in a slow rising and long lasting hyperpolarization in the second mitral cell [80, 98, 33, 48]. There is a variable delay between the evoked IPSC's in the second mitral cell and the spike times in the first mitral cell [98]. Thus, the evoked IPSC's occur asynchronously [80, 98, 33], aperiodically [33] and the kinetics of hyperpolarization in an ensemble average of the evoked IPSC's show a slow rise time ($\approx 100 - 150$ ms) and a slow decay constant ($\approx 350 - 600$ ms) [98, 33, 80]. In addition, the peak amplitudes of the ensemble average are small, (≈ 0.4 mV) [98]. The prolonged, asynchronous barrages of IPSC's have been shown to be a result of long latency, asynchronous and long lasting mitral cell recruitment of granule cells [48]. Furthermore, recent experimental studies into the origin of synchrony between mitral cells suggests that recovery from shared IPSC inputs from common granule cells is the primary driving mechanism for mitral cell synchrony [82, 33]. These physiologically measured properties of mitral-granule cell interactions suggest a novel mechanism of synchronization of mitral cells in the olfactory bulb.

Previous studies have proposed that noise can synchronize oscillators [93]. For neurons to undergo such noise-induced synchronization they should be periodically firing and should have some shared fast fluctuations in their inputs. Recent studies on the mechanism of generation of synchronized oscillatory activity by long lasting asynchronous, aperiodic inhibition in the olfactory bulb have revealed exactly such a novel role for noise [33]. It was shown that two mitral cells firing in the gamma frequency range can undergo synchronization upon receiving common inhibitory input from granule cells. The degree of synchronization was shown to depend on the degree of correlation in the noisy input shared by the two neu-

rons. Although spiking was synchronized, the shared noise itself was aperiodic. In all of the experimental and theoretical studies of stochastic synchronization to date, the degree of correlation is imposed and held fixed . In our study the degree of input correlation emerges intrinsically from within the network and is amplified over time due to the dynamics of the network. In addition, our study utilizes theoretically derived probability distribution of phase difference for uncoupled oscillators receiving shared noise to investigate the conditions necessary for the existence of bistability in the magnitude of input correlation. Here we consider the case in which correlated fluctuations from granule cells arise naturally from granule cells that connect to many mitral cells. The input correlation to any pair of mitral cells could increase if the shared pool of presynaptic granule cells increased their stochastic firing rate thus providing a greater amount of common noise. In the olfactory bulb, synapses between mitral and granule cells are dendrodendritic, and almost always reciprocal [45]. Thus, if a granule cell synapses on a pair of mitral cells, those mitral cells also synapse on that granule cell. We hypothesize that, since a pair of mitral cells with correlated input is more likely to fire synchronously, this pair is also more likely to provide correlated input to their common granule cell. In turn the common granule cell could then increases its release of transmitter increasing the correlation to the mitral cells. The result of this is that the feedback provides an amplification of correlation. The goal of this paper is to use computational and analytic techniques to show that such feedback will increase correlation and as a consequence, synchrony between oscillating mitral cells.

We describe three models for feedback induced correlation and stochastic sychronization. We first study one pair of mitral cells and one common granule cell. The mitral cells are modeled as simple phase oscillators which are perturbed through their phase-resetting curves (PRCs). The granule cell is modeled as a noisy leaky integrate and fire (LIF) neuron receiving synaptic input from the mitral cell oscillators. The second model replaces each phase oscillator with the conductance-based Morris-Lecar oscillator. Finally, to allow for analytic approaches, we reduce the first two models to a discrete time map which we study using an averaging technique.

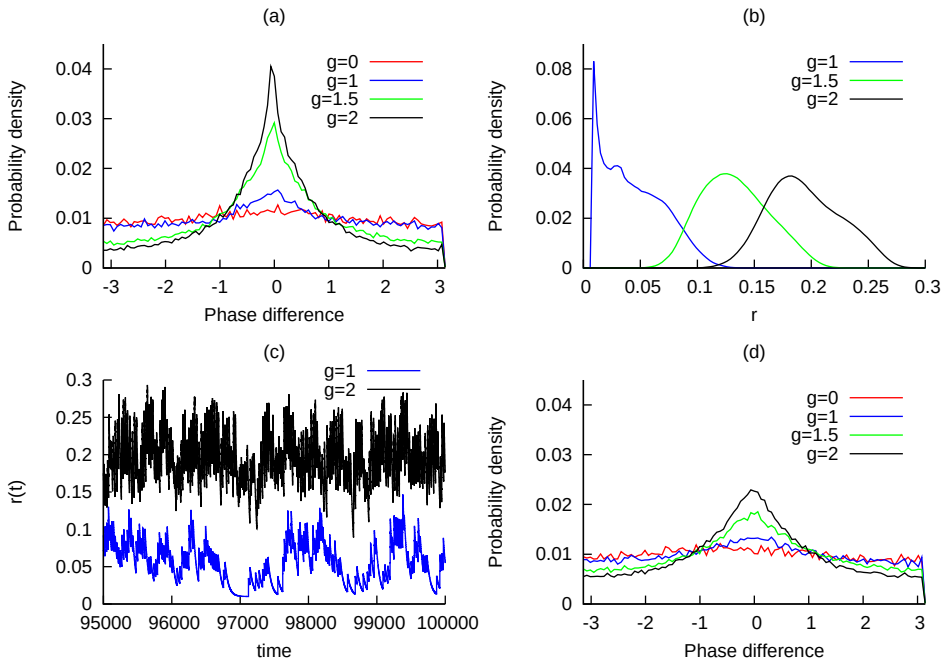

Figure 12: Self-organized synchronization in a stochastic feedback network of two mitral cells and one granule cell. (A) Probability density of the phase-difference $\phi = \theta_2 - \theta_1$ for different strengths of input to the granule cell. (B) Distribution of the values of r, the shared Poisson rate of the granule cell. (C) Plots of $r(t)$ for $g = 1$ and $g = 2$. (D) Phase difference histograms for the $3 + 3$ network.

3.2 RESULTS

3.2.1 "Spiking" Models

During odor inputs or stimulation, mitral cells fire in a narrow frequency range, so that we can regard them as limit cycle oscillators [62]. Any oscillator can be represented by a single phase variable [54], so we first consider a such pair of mitral cells as phase oscillators:

$$\frac{d\theta_i}{dt} = \omega_i$$

where ω_i is the natural frequency of the oscillator. These oscillators receive input from a shared granule cell which is modeled here as a noisy leaky integrate-and fire (LIF) neuron:

$$\tau \frac{dV}{dt} = -V + g(s_1 + s_2) + \sigma\xi(t).$$

$\xi(t)$ is a white-noise process and $s_i(t)$ are the synaptic inputs from the two mitral cells:

$$\frac{ds_i}{dt} = -s_i/\tau_s.$$

Each time θ_i crosses 2π, the synaptic input, s_i is incremented by 1. To model the long-lasting synaptic bombardment by the granule cell, we introduce a variable, r which satisfies

$$\frac{dr}{dt} = -\epsilon(r - r_0).$$

Each time the granule cell fires (V crosses its threshold, here set to 1), r is incremented by $\mu(r_{max} - r)$ and V is reset to 0. r represents the rate of the shared Poisson process. This shared Poisson process represents the feedback via dendrodendritic synapses from the population of granule cells to the mitral cells, the rate of which is dependent on the spiking activity of the granule cells. In addition, there are two independent Poisson processes (independent sources of noise) with fixed rates, r_1, r_2. Each of these three Poisson processes generates events which we regard as the brief random inhibitory post synaptic potentials seen in patch clamped mitral cells [82]. We suppose that the effect of these inputs on the mitral cell oscillator is to shift the timing of the next mitral cell spike by an amount that depends on its current phase. The function that determines this shift is called the *phase resetting curve*, denoted, $\Delta(\theta)$ which has been computed for many types of neural oscillators, including mitral cells [30]. If oscillator j receives an input, then its subsequent phase (and thus timing) is given by, $\theta_{new} = \theta_{old} + \alpha\Delta(\theta)$, where α is the magnitude of the kick. If the input is generated by the shared process with rate r, both $\theta_{1,2}$ are incremented while if the event is generated by the process with rate r_i, only oscillator i is incremented. In our simulations, we choose $\omega_i = 2\pi/25, \tau = 1, \tau_s = 4, r_{max} = 0.5, \mu = .05, \sigma = 0.2, r_{0,1,2} = 0.01, \epsilon = .02$, $\Delta(\theta) = -\sin\theta$ and $\alpha = 0.5$. We vary the coupling, g to the granule cells from the mitral cells between 0 and 2. We will refer to the above network construction (2 mitral cells and 1 granule cell) as the $2 + 1$ network. We also made a network consisting of three oscillators

(mitral cells) and three granule cells (LIF). Oscillators 1,2 drove LIF 1, 1,3 drove LIF 2, and 2,3 drove LIF 3. Oscillator 1 received Poisson input from LIF 1,2; 2 from 1,3; and 3 from 2,3. All other parameters are the same. This network will be referred to as the $3+3$ network as depicted in Figure 3.2.1.

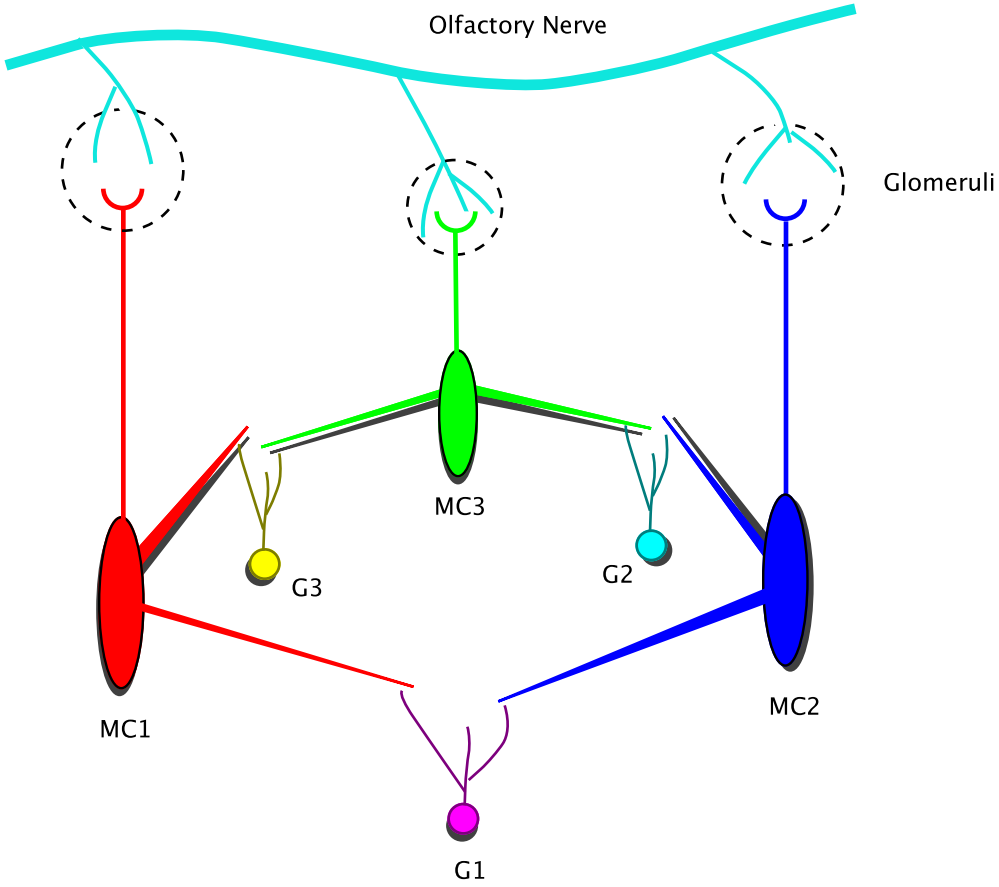

Figure 13: **Schematic depicting the network architecture** The generalized $(3+3)$ network with 3 mitral cells and 3 granule cells is shown here. The simplified $(2+1)$ network lacks mitral cells (MC3).

There are several ways to quantify synchrony in oscillator networks. For phase models in which the phase is explicit, it is convenient to look at the histogram of the phase-differences, $\theta_2 - \theta_1$; the more peaked is this histogram, the closer to perfect synchrony ($\theta_1 = \theta_2$) are the two oscillators. Figure 3.1 depicts simulations of the $2+1$ network. Figure 3.1A shows a histogram of the phase-differences, $\theta_2 - \theta_1$ as a function of the coupling from the mitral cells

to the granule cells. When the LIF granule cell is uncoupled from the mitral cells, $g = 0$, the histogram is nearly flat as the rate of shared input is the same as the unshared input and both are quite low. There is a small peak due to the small degree of correlation. As the coupling to the granule cell increases, the peak of the histogram becomes much sharper since the firing of the granule cell is now dependent on the spiking of the mitral cells. As a consequence of this sharpening, the rate of the shared input, r increases as shown in the histograms of Figure 3.1B for identical values of g. It is important to understand that the firing rate of the shared granule cell population, r indicates the input correlation in the mitral cells that share these granule cells, which in turn represents the magnitude of synchronization of these mitral cell activities. Hence we use r as a stand-in for synchronization in the mitral cells. The probability distribution of r can also depict the stability of the input correlation (and hence synchronization) in the system. If the distribution is bimodal it indicates the existence of bistability in the input correlation in the mitral cells (and their synchronization). Thus in Figure 3.1B, $g = 1$ is interesting since it appears to be slightly bimodal, i.e. the distribution of r has two peaks for $g = 1$. Figure 3.1C shows a segment of the temporal dynamics of r for $g = 2$ and $g = 1$. Figure 3.1D shows a simulation of the 3 mitral and 3 granule cell network. The peaks are not as sharp as in Figure 3.1A for similar input strengths. This is because oscillator 1 gets two strong inputs from granule cell 1 and granule cell 2 and thus shares correlations with the *two* other mitral cells putting a limit on the maximum correlation from a single cell.

In Figure 3.1, we modeled the "mitral" cells as a pair of simple phase models. There is similar behavior when we replace the phase oscillators with conductance-based models such as the Morris-Lecar model but with very pronounced bistability. Figure 3.2.1 shows a sample simulation with the same set up as in Figure 3.1, but the phase models are replaced by the Morris-Lecar oscillator. Since phase is difficult to obtain, we instead look at the correlation between the voltages over a moving time window (see methods). There appears to be two "attractors"; one where the oscillators are completely uncorrelated and r is low and the other when they are tightly correlated and r is high. This is suggestive of the possibility of bistability. Figure 3.1C ($g = 1$) shows a similar bistability between the synchronized and desynchronized state. We suspect that intrinsic noise in the system effects the switch from

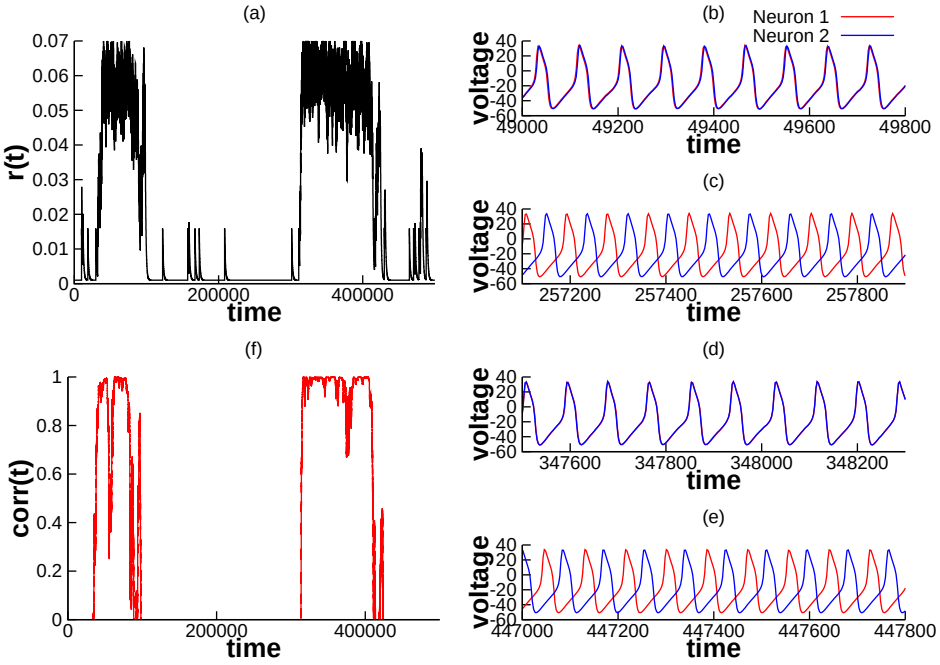

Figure 14: Self-induced stochastic synchrony between a pair of Morris-Lecar model neurons and a leaky integrate-and-fire model neuron. (A) Rate of release of the LIF, "granule cell" showing switches between synchrony and asynchrony. (B-E) Sample voltages at four different time points corresponding to time in A, showing synchrony when $r(t)$ is high and asynchrony when $r(t)$ is low. (F) Correlation coefficient calculated for the voltage data between the two mitral cells

one to the other and the positive feedback maintains the states for a long period of time.

We can begin to understand the mechanism of amplification of synchronization by considering the dynamics of r. We suppose that ϵ, μ are small so that we can average r and see that its value depends on the firing rate, F of the LIF:

$$\frac{dr}{dt} = -\epsilon(r - r_0) + \mu F(r_{max} - r) \tag{3.1}$$

Figure 3.2.1 shows how the LIF firing rate, F, depends on the phase difference between the two oscillators, ϕ. Here we count the number of spikes in a time window of 10 seconds to determine F. The shape of this function depends on g, the time constant of the synapse, τ_s (as well as other parameters such as τ and σ.) In general, this is a decreasing function of ϕ. As the strength of the synapse, g increases or as the decay of the synapse, τ_s increases, the spike count is larger and depends less on the phase-difference between the oscillators. For small g and short-lasting synapses, the LIF is a coincidence detector and depends very strongly on the timing difference of the inputs. Thus, for $g = 1, \tau_s = 2$, if the phase difference between the two oscillators is more than about 0.75 radians (corresponding to about 3 msec for oscillators running at 40 Hz) then there will be almost no firing of the LIF. Similarly, for $g = 2, \tau_s = 1$, (green), the timing difference should be less than 6 msec. For larger g and longer synapses, the LIF always fires and the ratio of the minimum to the maximum rates is only modestly small.

We can now see the basic principles underlying the amplification of stochastic synchronization. Initially, r is low and the shared granule cell fires at a very low frequency. The phase difference between the two oscillators drifts, and thus, on occasion the two mitral cells fire nearly synchronously. This increases r transiently and thus increases the correlation of the inputs to the oscillators. This in turn increases the rate at which the shared granule cell fires, further increasing r resulting in a positive feedback loop and finally mitral cell synchronization. In the next section we derive a more abstract model which we are able to analyze.

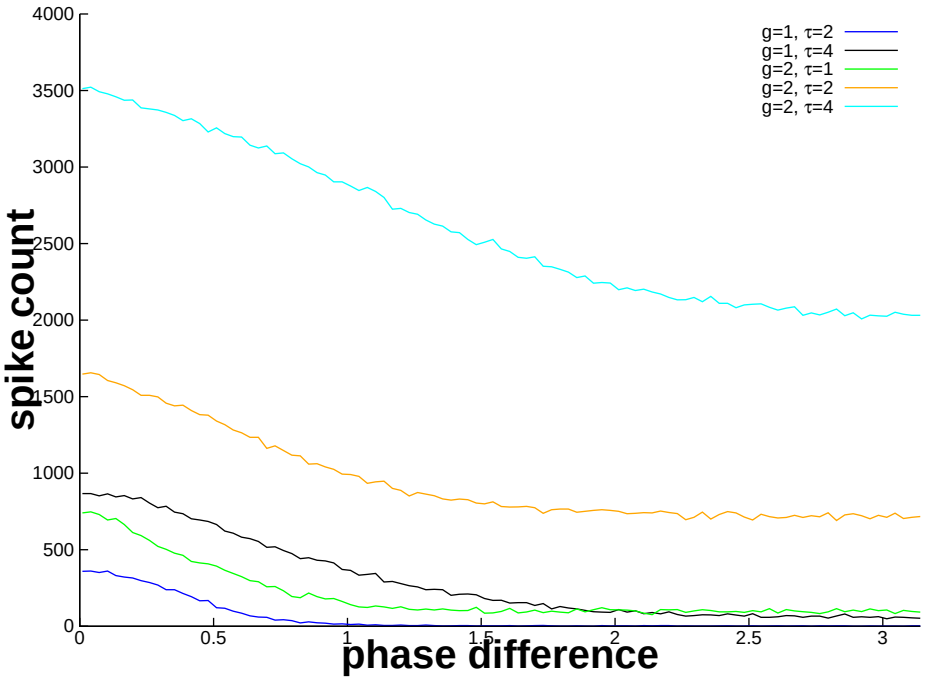

Figure 15: Dependence of the total spike count of the granule cell on the phase-difference of the two oscillators for different input strengths (g) and integration times of the synapse (τ_s).

3.2.2 Reduced Model

We start with exactly the same model as above for the mitral cells: a pair of phase oscillators. However, instead of explicitly modeling the LIF and its synaptic excitation we consider only the r equation (3.1) which will be incremented according to the degree of synchronization of the two mitral cells. That is, we replace F by an explicit functional of the phase-difference between the two oscillators. As above r sets the rate of a Poisson process that produces events which excite *both* mitral cell oscillators. Similarly, there are two independent processes with fixed rates $r_{1,2}$ which provide background unshared noise to the two mitral cell oscillators. Let T_n be the time interval between events for these three Poisson processes. We choose T_n from an exponential distribution with rate $r + r_1 + r_2$ and then choose which of the three events has occurred according to the relative sizes of r, r_1, r_2 (as per the Gillespie algorithm [34]). We can then reduce the behavior of the randomly perturbed oscillators to a map and thus use the theory developed in [61] to determine the density of the phase-differences. Specifically, let $\Theta_j^{(n)}$ denote the phase of oscillator j after the n^{th} kick from a population of granule cells (common and independent projections). Then

$$\Theta_1^{n+1} = \Theta_1^n + T^n\omega + c_1\Delta(\Theta_1^n) \tag{3.2}$$

$$\Theta_2^{n+1} = \Theta_2^n + T^n\omega + c_2\Delta(\Theta_2^n). \tag{3.3}$$

$c_j = \alpha$ if oscillator j is kicked and is zero otherwise. Thus, if the event was generated by the common process with rate r, $c_1 = c_2 = \alpha$, while if it was generated by the independent process, say, r_1 then $c_1 = \alpha$ and $c_2 = 0$. These equations simply say that the phase of each oscillator at the $n + 1^{th}$ granule cell spike is equal to the phase at n^{th} granule cell spike advanced by the phase traversed by the oscillator given its angular frequency ω in the n^{th} inter-spike interval T_n. If the oscillator receives the n^{th} granule cell spike ($c = 1$), an additional phase advance/delay dictated by the phase resetting curve, $\Delta(\Theta^n)$ is added to obtain the actual phase of the oscillator at the $n + 1^{th}$ granule cell spike, Θ_j^{n+1}. The probability of both oscillators receiving granule cell input simultaneously ($c_1 = 1$,$c_2 = 1$) is $p = r/(r + r_1 + r_2)$. The probability of either one of the oscillators receiving granule cell input ($c_1 = 0$, $c_2 = 1$) and ($c_1 = 1$, $c_2 = 0$) is thus $\frac{(1-p)}{2}$. To simulate this process, we

generate two random variables, one to determine the interval between inputs, T_n drawn from an exponential distribution and the other drawn from a uniform distribution to determine which of the three pairs, $(c_1, c_2) \in \{(1,1),(1,0),(0,1)\}$ occurs.

In a previous study [61], p was assumed to be constant. Here, since p is proportional to the rate of the common granule cell which is, in turn, proportional to the degree of synchronization of the mitral cells, we allow p to evolve on a slow scale similar to equation (3.1):

$$p^{n+1} = p^n + \epsilon[(P_{min} - p^n) + \Gamma(\Phi^n)(P_{max} - p^n)] \tag{3.4}$$

The functional Γ could depend on the instantaneous phase-difference between the mitral cell oscillators $\Phi^n = \Theta_1^n - \Theta_2^n$ or some time averaged version of it. We discuss several choices in the next section. However, we assume that Γ gets larger when the two oscillators are more synchronous (Φ^n near zero) and small when they are not synchronous. Thus, when Γ is large ($\Gamma \gg 1$), p_n will slowly evolve toward P_{max} while when Γ is small ($\Gamma \ll 1$), it will decay toward P_{min}. In terms of the original models with the LIF, $P_{min,max} = r_{min,max}/(r_{min,max} + r_1 + r_2)$.

3.2.3 Choice of $\Gamma(\Phi)$:

There are at least two plausible ways to choose Γ a direct and indirect way. In the direct way, we assume that Γ is a function of Φ^n, while in the indirect version, Γ is a function of some time averaged version of the phase-difference, such as an order parameter. We will discuss the direct choice first.

3.2.3.1 Single stable fixed point Figure 3.2.1 shows how the firing rate of the "granule cell" depends on the phase-difference Φ. The probability of shared input is proportional to this rate, so a natural choice for Γ is proportional to the firing rate $F(\Phi)$ depicted in the figure, for example, $\Gamma(\Phi) = K[F(\Phi)/F_{max}]^M$. If M is large, this creates a highly peaked function of the phase difference with a maximum at zero. We use the following approximation of such a function:

$$\Gamma(\Phi) = Ke^{-M(1-\cos(\Phi))}$$

With this choice for Γ, equations (3.2, 3.3, 3.4) constitute a simplified discrete dynamical system to represent the models from Figures 3.1 and 3.2.1. Figure 3.2.3.1A shows the evolution of p_n over time with $\epsilon = 0.0005, K = 6, P_{min} = 0.1, P_{max} = 1, M = 15, \Delta(x) = -0.25\sin(x)$. After a long transient, the stochastic variable, p_n tends to a fairly sharp density function centered around $p = 0.7$ (see Figure 3.2.3.1B). At the same time, the phase-difference, Φ_n evolves on a fast scale to a highly peaked distribution centered at $\Phi = 0$ as shown in Figure 3.2.3.1D. Here, we let the oscillators evolve according to equations (3.2, 3.3) for T iterations. We see that in the early stages, the density of phase difference is flat but becomes peaked as the simulation evolves in time. We can vary the magnitude of the function Γ, α and examine the steady-state value of p_n. This is shown in Figure 3.2.3.1C. In order to analyze this equation, we exploit the assumption that ϵ is small. Since ϵ is small, we can apply averaging and approximate the dynamics of p_n by the dynamics of the averaged equation, q_n satisfying:

$$q^{n+1} = q^n + \epsilon[(P_{min} - q^n) + \langle\Gamma(\Phi^n)\rangle(P_{max} - q^n)], \tag{3.5}$$

where $\langle\Gamma(\Phi^n)\rangle$ is the average value of $\Gamma(\Phi^n)$. In order to calculate $\langle\Gamma(\Phi^n)\rangle$, we require $P(\Phi^n, q^n)$, which is the probability density of phase difference Φ^n given q^n. Since q^n evolves slowly, we can treat it as constant allow the oscillators to evolve until they reach a stationary density. In [61], we obtain an analytic formula for the steady state density, $P(\Phi, p)$, the density of phase-differences, Φ given a probability, p of common input. From this, we obtain:

$$\langle\Gamma(\Phi^n)\rangle = \int_0^{2\pi} P(\Phi, q^n)\Gamma(\Phi)d\Phi \equiv \gamma(q^n). \tag{3.6}$$

Hence, we can analyze this case by finding the stable fixed points for the averaged dynamics:

$$q^{n+1} = q^n + \epsilon[(P_{min} - q^n) + \gamma(q^n)(P_{max} - q^n)].$$

The fixed points satisfy:

$$\gamma(q) = \frac{q - P_{min}}{P_{max} - q}$$

$\gamma(q)$ is typically a bounded non-negative increasing function of q. The right-hand side less than or equal to zero at $q = 0$ and has a vertical asymptote at $q = P_{max} < 1$, so that there

is always at least one stable fixed point between 0 and 1. For our simple choice of Γ there is exactly one stable fixed point for q^n. In Fig 3.2.3.1A, the model was allowed to evolve from random, uniformly distributed initial phase difference between the two oscillators and various uniformly distributed initial values for q^n. It is seen that irrespective of the initial conditions, the system evolves towards a single stable fixed point for q^n. The theoretically predicted value of the stable fixed point agrees well with the median of the distribution of the steady state q^n values from many trials, as seen in Figure 3.2.3.1B. The green curve shows the function,

$$f(q) = P_{min} - q + \gamma(q)(P_{max} - q). \tag{3.7}$$

The position of the stable fixed point for q^n depends on the magnitude of α. At small values of α, the steady state lies close to P_{min}. For larger values of α, the steady state q^n increases monotonically towards P_{max}. The predicted steady state values match well with Monte-Carlo simulations as can be seen in Figure 3.2.3.1C. In Figure 3.2.3.1D, it can be seen that the evolution of synchrony evolves over time over a time scale of 100 ms, as can be observed from the distribution of phase difference at different points during the simulation.

Before moving to the next section, we can ask whether or not there is more than one stable fixed point to the averaged dynamics. We conjecture that there will not be. The reason for this is that in [61], we show that the probability density, $P(\Phi, q)$ has the form:

$$P(\Phi, q) = \frac{N}{1 - \frac{2q}{1+q}\frac{h(\Phi)}{h(0)}}$$

where $h(\Phi)$ depends on the shape of the PRC, $\Delta(\theta)$. Integrating P against $\Gamma(\Phi)$ yields a function of q which for small q depends linearly on q and saturates to $\Gamma(0)$ as $q \to 1$ (since P approaches a delta function). Thus, $\gamma(q)$ is roughly like

$$\gamma(q) \approx \frac{A + Bq}{C + Dq}$$

with A, B, C, D positive no matter how we choose $\Gamma(\Phi)$. For this approximation, it is easy to show that $f(q)$ has at most one positive root. Thus, we expect no bistability between a synchronous and an asynchronous state. In order to get bistability, there should be an inflection point $\gamma(q)$, for example by having $\gamma(q)$ depend sublinearly on q for q small, e.g., $\gamma(q) = Aq^2$ for small q. We will study a choice of Γ that produces bistability in the next section.

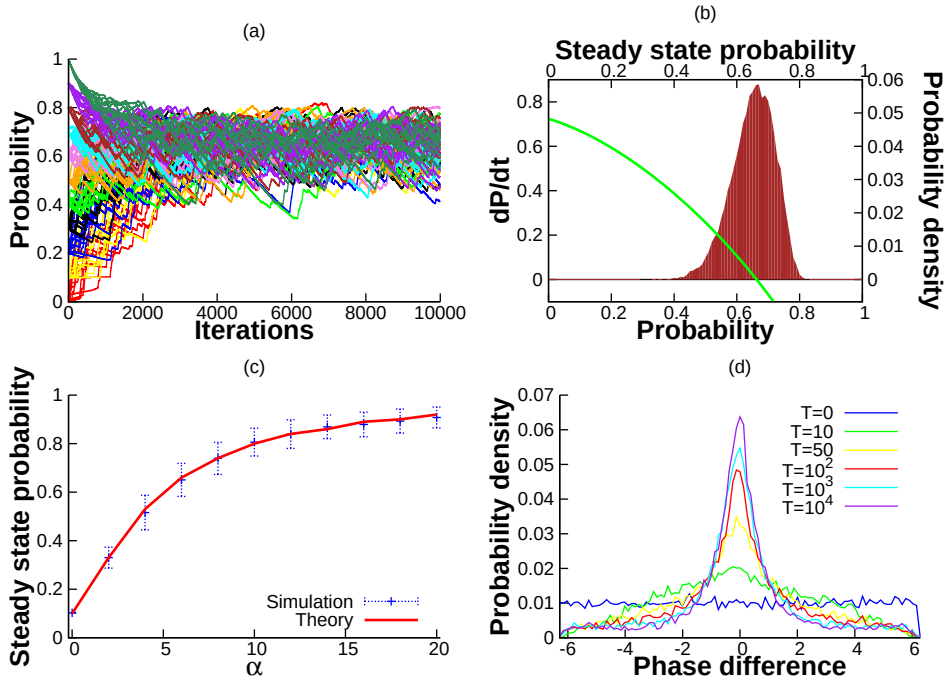

Figure 16: Evolution of p in the presence of a single stable fixed point. (A)The temporal evolution of p from various initial states. All initial states are attracted by the single stable fixed point. (B) Histogram of the final values of p in different trials from (A). The green curve depicts the numerically calculated values of equation 3.7 (C) The dependence of the median steady state probability on the amplitude of α. (D) Sharpening of the probability distribution of the phase difference between mitral cells in time. The time points represent number of iterations as in (A)

3.2.3.2 Bistability When Γ is an *instantaneous* function of Φ, then there appears to be no bistability between asynchrony and synchrony. To produce a model which exhibits the kind of bistability shown in the full model (e.g. Figure 3.2.1A,B), we will assume that Γ is a function of some temporal average of the phase difference. That is, instead of averaging over a nonlinear function of the phase, we apply a nonlinear function *after* performing some averaging. Before discussing how such a rule could be biologically implemented, we consider a simple choice for this rule. A common measure of synchrony [54, 61] is the circular variance (or "order parameter"):

$$Z := \sqrt{\langle \cos \Phi_n \rangle^2 + \langle \sin \Phi_n \rangle^2}$$

We can write this order parameter as a function of the of the density, $P(\Phi, p)$:

$$Z(p) = \int_0^{2\pi} \cos \Phi P(\Phi, p)\ d\Phi$$

since P is an even function of Φ and in our previous work [61], we showed that $Z(p) \approx bp$ for p small; that is, it is linear. The results in the previous section show we need nonlinear dependence on p, so we take

$$\Gamma = Z^2$$

which will give us p^2 dependence for p small.

This choice of Γ produces a fundamental change in the system's dynamics. The system with, $\epsilon = 0.01, \alpha = 10, p_{min} = 0, p_{max} = 1, \Delta(x) = \sin(x)$, now displays two distinct stable states as seen in Fig 3.2.3.2(a), where the system with random uniformly distributed initial phase difference and q^n evolves either to a zero or a non-zero steady state q^n. The steady state distribution of q^n values reveals the two stable fixed points as seen in Fig 3.2.3.2b, both of which are predicted accurately by theory. The position of the non-zero stable state depends on the choice of α. Fig 3.2.3.2(c) shows the agreement between the theoretically predicted value, the mean of the distribution of all final states higher than the unstable fixed point and the position of the peak in the distribution of the non-zero steady states. Finally, the two stable states differ in their synchronization. The zero stable state is characterized by oscillators with low synchrony whereas the non-zero stable state has oscillators with significantly higher synchrony as can be seen in Fig 3.2.3.2(d).

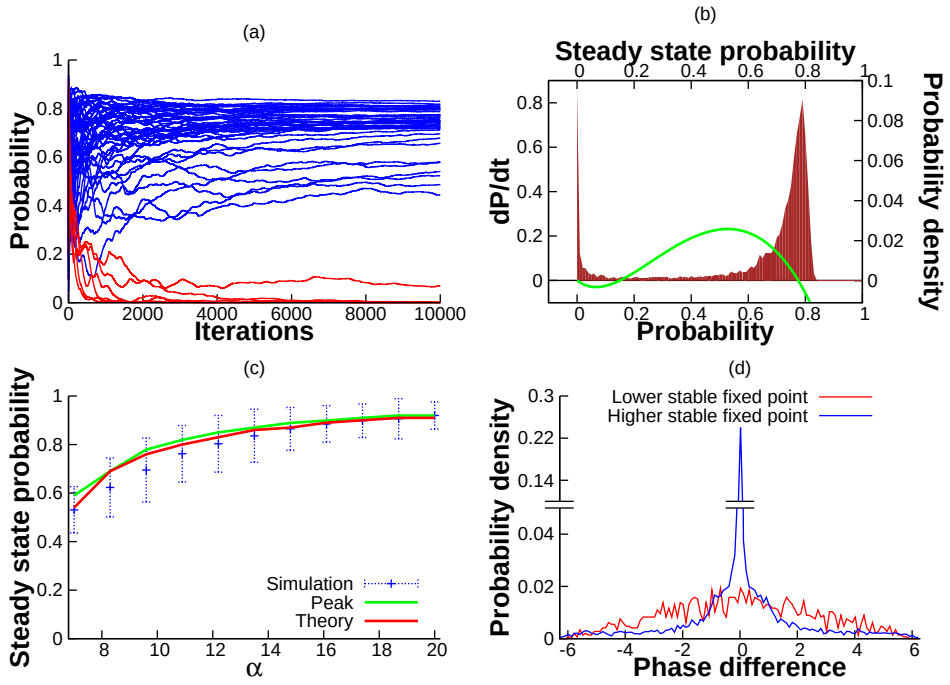

Figure 17: Evolution of p in the bistable regime. (A) The temporal evolution of p from various initial states. The initial states move randomly to either one of the stable fixed points. (B) Histogram of the final values of p in different trials from (A). The green curve depicts the numerically calculated values of equation 3.7 for the indirect choice of Γ. (C) The dependence of the steady state probability on the amplitude of α. The taller peak of the bimodal distribution is depicted by the green curve. (D) Probability distribution of the phase difference between mitral cells for the two fixed points.

This choice of Γ produces a fundamental change in the system's dynamics. The system with, $\epsilon = 0.01, \alpha = 10, p_{min} = 0, p_{max} = 1, \Delta(x) = \sin(x)$, now displays two distinct stable states as seen in Fig 3.2.3.2(a), where the system with random uniformly distributed initial phase difference and q^n evolves either to a zero or a non-zero steady state q^n. The steady state distribution of q^n values reveals the two stable fixed points as seen in Fig 3.2.3.2b, both of which are predicted accurately by theory. The position of the non-zero stable state depends on the choice of α. Fig 3.2.3.2(c) shows the agreement between the theoretically predicted value, the mean of the distribution of all final states higher than the unstable fixed point and the position of the peak in the distribution of the non-zero steady states. Finally, the two stable states differ in their synchronization. The zero stable state is characterized by oscillators with low synchrony whereas the non-zero stable state has oscillators with significantly higher synchrony as can be seen in Fig 3.2.3.2(d).

3.3 DISCUSSION

We have described a new mechanism for the amplification of oscillatory synchrony through feedback. Unlike previous models that depend on phasic oscillatory inhibition [9], our feedback is long-lasting (nearly tonic) and highly stochastic. Specifically, we study stochastic synchronization in a generalized network of mitral cells by inhibitory granule cell inputs which themselves receive dendrodendritic mitral cell feedback. The mitral cells are not directly (monosynaptically) coupled but are coupled disynaptically via the shared granule cells. Thus, the granule cells provide both the recurrent and lateral connectivity, as has been described in the mammalian olfactory bulb. We use spiking models with LIF neurons to demonstrate the feasibility of stochastic synchronization in the olfactory bulb with feedback from granule cells. We then use abstract models to analyze the mechanism of the self-organization as a result of the feedback-induced stochastic synchronization. Our models are based on experimentally observed kinetics of the mitral-granule cell interaction's. The key assumptions of our model, borne out in experimental studies are that the granule cell output consists of asynchronous, aperiodic, prolonged barrages of IPSC's with small average

amplitudes and long ensemble decay constants. Such mitral-granule cell interactions have been observed experimentally using extracellular stimulation in the glomerular layers as well as intracellular stimulation of mitral cells [80, 98, 33, 48, 82].

Fast synchronized inhibition has been shown to play a central role in producing synchronization in a sparse, randomly connected network of excitatory and inhibitory cells where the PING (pyramidal interneuronal network gamma) mechanism is observed [9]. However, in the olfactory bulb, mitral cells receive inhibitory postsynaptic potential (IPSC's) from granule cells in the form of asynchronous barrages with small average amplitudes [98]. In addition, the decay time constant of the probability envelope of these IPSC's is too long [98, 82, 33], for a PING-like mechanism to produce synchrony [101]. PING is based on fast inhibitory feedback which produces a "window of opportunity" for the excitatory cells to fire and thus requires strong inhibition. The synchrony induced by stochastic synchrony is not locked to the inhibitory events, but instead relies on the correlations in the "noisy" granule cell inputs shared by mitral cells. Here, we study the role of feedback in this system. Specifically, we propose that more synchronous mitral cell activity could produce activity of shared granule cells which would result in higher correlations in the input to the mitral cells. In other words, we propose a positive feedback loop in which the stochastic synchronization of mitral cells is enhanced by the correlated inhibitory output from granule cells, which in turn is enhanced by the correlated mitral cell spiking. As the synchrony is dependent on correlation of input from shared granule cells rather than fast transient inhibition, it is a distinct and separate mechanism from PING.

Olfactory bulb circuitry is unique in the central nervous system. The principle output cells, mitral cells, make synapses with the inhibitory granule cells through their dendrites rather than their axons. Activity of the granule cells produces long lasting recurrent and lateral inhibition which has two components: a long lasting slow component and a fast random component. The slow component acts to keep the spike frequency of the mitral cells in a limited range i.e. the firing rate of the mitral cells does not vary much with odor concentration [62], thus the slow asynchronous inhibition acts to balance the excitatory drive to the mitral cells. The fast component serves as "correlated noise" to synchronize mitral cell oscillations. Granule cells do not need to spike to produce inhibition , thus, with weak

stimulation, effects of inhibition remain local and provide little correlation between mitral cells. However, if several mitral cells fire together, then this may be enough to cause the shared granule cell to fire spikes resulting in the widespread calcium release into granule cell dendrites and thus, all the mitral cells that are connected to that particular granule cell will receive fast correlated random inhibitory input [82] which results in lateral inhibition.

In the spiking model, we use a slow variable $r(t)$ to describe a shared Poisson process whose rate is modulated by the spiking of the single common granule cell in the $2+1$ model. This process is used to mimic a population of common granule cells whose firing rates are modulated by synchronized firing of the mitral cells. This simplification is used in order to obtain a probability envelope of an ensemble average of shared granule cell inputs where individual granule cells are assumed to be Poisson processes. We show in the spiking model that stochastic synchronization can indeed be induced by the feedback loop between the mitral and granule cells.

We show that in the abstract model using general oscillators that a feedback loop between mitral and granule cell input can indeed synchronize mitral cell activity which is otherwise uncorrelated. The abstract model also provides important insight into the nature of dependence of the evolution of p on the phase difference, Φ between the oscillators. Dependence of Φ on a centrally peaked Γ, produces a system with only one stable steady state. On the other hand, if Γ is an order parameter, then bistability between synchrony and asynchrony is possible in some parameter regimes. The spiking network also displays similar dependence on granule cell activity. Both the abstract and spiking models show a gradual temporal evolution of synchrony which is similar to observed evolution of synchrony in the olfactory bulb(see figure 2A in [82]). The Morris-Lecar model suggests the existence of bistability, even though the granule cell rate is dependent on the *instantaneous* (as opposed to time averaged) timing difference between the two mitral cells. This could be a consequence of the fact that the synapses to the mitral cell oscillators have temporal dynamics rather than being instantaneous. Interestingly experimental observations of desynchronized to synchronized shifts of mitral cell activity and vice versa [82] (see figure 2C) seem to suggest the possibility of bistability in the input correlation (and synchrony of mitral cells) in the olfactory bulb. We conjecture that in the olfactory system, the mitral-granule network

is monostable. But, if bistability should indeed exist, it would most probably be mediated by a slow process that accumulates coincident activity of mitral cells over time. Bistability might be common place in other cortical networks where such memory forming slow cellular processes might have evolved. In such networks, a transient increase in correlated inputs can push the system from one state to another, hence allowing for a transient correlation-induced dynamic switching behavior. Evoked IPSC's in a lateral mitral cell are known to occur with a variable latency [98]. Granule cell activity is also known to develop with a variable long-latency [48]. In addition, synchrony between mitral cells is known to develop with a variable delay (50-150ms) [82]. These latencies are thought to be a function of the stereotypical fashion in which mitral cells recruit granule cell activity and in turn experience a shaping of their own activities. Our models did not include detailed cell type specific morphologies but could reproduce the time dependent evolution of synchrony between mitral cells (see Figure 3.2.3.1D).

Both the simple and generalized network models have a notable dependence of their synchronization on the rate of decay of p. Finally, it can be seen that the phase difference of two mitral cells is highly dependent on the firing rate of the granule cell. These results taken together suggest that stochastic synchronization does play a major part in determining the activity of a network of mitral and granule cells in a closed loop with feedback connectivity. Although this investigation focuses on specific details of the olfactory circuit, the proposed mechanism is generally applicable to cortical circuits that include a subpopulation of neurons that provide long lasting, small amplitude, asynchronous outputs.

3.4 METHODS

3.4.1 Morris Lecar Model

We used the general Morris-Lecar model with the following equations.

$$C\frac{dV_i}{dt} = I - g_{ca}m_{\infty,i}(V_i - V_{Ca}) - g_k w_i(V_1 - V_K) - g_l(V_i - V_l) - g_{syn}s_i(V_1 - E_r))$$

$$\tau_{w,i}\frac{dw_i}{dt} = \phi(w_{\infty,i} - w_i)$$

$$m_{\infty,i}(V) = \frac{1}{2}(1 + \tanh((V - V_a)/V_b))$$

$$w_{\infty}(V) = \frac{1}{2}(1 + \tanh((V - V_c)/V_d))$$

$$\tau_{w,i}(V) = \frac{1}{\cosh((V - V_c)/(2V_d))}$$

$$\tau_s\frac{ds_i}{dt} = -s_i$$

with parameters, $g_{Ca} = 4.4, g_k = 8, g_l = 2, g_{syn} = .1, E_r = -70, V_k = -84, V_l = -60, V_{Ca} = 120, V_a = -1.2, V_b = 18, V_c = 2, V_d = 30, \phi = .04, \tau_s = 5, C = 20$.

To compute the correlations shown in Figure 3.2.1, we compute

$$x_{ij}(t)\frac{1}{T}\int_{t-T}^{t}(V_i(s) - \overline{V})(V_j(s) - \overline{V})\ ds$$

and plot $x_{12}(t)/\sqrt{x_{11}(t)x_{22}(t)}$.

4.0 RATE OF CONVERGENCE OF STOCHASTIC SYNCHRONY

4.1 INTRODUCTION

The closed-form solution obtained in equation 2.9 in chapter 2 was used to the steady-state probability density of phase differences. This was instructive in understanding the dependency of the output correlation on PRC-type membership. But in addition to the steady-state, the temporal evolution of the system i.e. the speed with which the system relaxes to the steady-state density is also of interest. Since the operator in equation 2.9 has an eigenvalue of 1 corresponding to the steady-state solution, the second largest eigenvalue determines the rate of convergence to the steady-state solution. The theoretical question of interest is the relationship between the eigenvalues and the PRC-type. We aim to to derive an expression for the eigenvalues as a function of the PRC.

4.2 SIMPLIFYING THE PROBLEM

In order to obtain the eigenvalues we will utilize our repertoire of perturbation methods. Our choice of the perturbation technique depends crucially on the fact that we are only interested in the eigenvalues that are large. Specifically we will use the WKB (Wentzel-Kramers-Brillouin) method named after the physicists Gregor Wentzel, Hendrik Anthony Hans Kramers and Leon Nicolas Brillouin who developed the method. In general, the method is used for approximating the solution of a differential equation whose highest derivative is multiplied by a small parameter [8].

In order to obtain the eigenvalues of the system,

$$\frac{\partial p(x,t)}{\partial t} = \frac{\partial^2}{\partial x^2}[p(x,t)G(x)] \tag{4.1}$$

we employ a common technique of solving partial differential equations assuming separability of the solution into two functions that are dependent only on one of the variables. If we now assume that $p(x,t) = \Phi(x)T(t)$, i.e. it is separable, then equation 4.1 can be written as,

$$\Phi T_t = \Phi_{xx} TG + 2\Phi_x TG_x + \Phi TG_{xx} \tag{4.2}$$

which can then be separated as,

$$\frac{T_t}{T} = \frac{\Phi_{xx} G}{\Phi} + \frac{2\Phi_x G_x}{\Phi} + G_{xx} = -\lambda \tag{4.3}$$

where $-\lambda$ is the separation constant and the negative sign is chosen for convenience. Thus we obtain two differential equations,

$$T_t + \lambda T = 0 \tag{4.4}$$

and

$$\Phi_{xx} G + 2\Phi_x G_x + \Phi G_{xx} + \lambda\Phi = 0. \tag{4.5}$$

Eq: 4.5 can be written as,

$$(\Phi G)'' + \lambda\Phi = 0 \tag{4.6}$$

If we let, $y(x) = \Phi(x)G(x)$, we can transform equation 4.5 to

$$y''(x) + \frac{\lambda}{G(x)} y(x) = 0. \tag{4.7}$$

Assuming $G(x)$ to be a purely positive function ($G(x) \geq 0$), we expect oscillatory solutions for equation 4.7. Then, denoting $K(x) = \sqrt{\frac{1}{G(x)}}$ and $\epsilon = \frac{1}{\sqrt{\lambda}}$, equation 4.7 can be written as,

$$\epsilon^2 y'' + K(x)^2 y = 0 \tag{4.8}$$

4.3 DERIVING THE WKB APPROXIMATION

Since we are interested in large eigenvalues of the operator in equation 4.1, we can reasonably make the assumption that ($\lambda \gg 0$) or ($0 < \epsilon << 1$). Now we can use the WKB approximation. This method is particularly suited for approximating large eigenvalues but works sufficiently well even if this condition is relaxed. Since $K(x)$ is positive we expect oscillatory solutions for equation 4.8 as. If $K(x)$ was just a purely positive constant ($K_0 > 0$), the solution for equation 4.8 is of the form $y(x) = e^{\frac{(iK_0x)}{\epsilon}}$. Since $K(x)$ is not a constant in our case, we can guess a solution of the form $y(x) = e^{\frac{iu(x)}{\epsilon}}$. This is similar to the technique of variation of parameters for finding solutions to general linear second-order differential equations. Then substituting this candidate solution into equation 4.8 we get,

$$i^2y(x)u'(x)^2 + i\epsilon y(x)u''(x) + K(x)^2y(x) \tag{4.9}$$

Dividing equation 4.9 by $y(x)$ and using the identity, $i^2 = -1$, we can simplify equation 4.9 to,

$$i\epsilon v' - v^2 + K(x)^2 \tag{4.10}$$

where $v = u'$. Then we can perform a regular perturbation expansion by expanding $v(x)$ in powers of ϵ by expressing $v(x)$ as,

$$v(x) = v_0(x) + \epsilon v_1(x) + \epsilon^2 v_2(x) + \mathcal{O}(\epsilon^2). \tag{4.11}$$

We can now substitute equation:4.11 into equation4.10 as follows,

$$\epsilon\Big[v_0'(x) + \epsilon v_1'(x) + \mathcal{O}(\epsilon^2)\Big] - \Big[v_0(x)^2 + \epsilon^2 v_1(x) + 2\epsilon v_0(x)v_1(x)\Big] + K(x)^2 \tag{4.12}$$

In order to perform the expansion, we rearrange equation 4.12, and collect the ϵ terms which gives us,

$$-v_0(x)^2 + K(x)^2 + \epsilon\Big[iv_0(x)' - 2v_0(x)v_1(x)\Big] + \mathcal{O}(\epsilon^2). \tag{4.13}$$

Thus we can solve for v_o, v_1 by observing that, at $\mathcal{O}(1)$, $v_0(x)^2 = K(x)^2$ and hence $v_0(x) = \pm K(x)$. At $\mathcal{O}(\epsilon)$ we get $-2v_0(x)v_1(x) = -iv_0(x)'$, therefore $v_1(x) = \frac{iv_0(x)'}{2v_0(x)} = \frac{iK'(x)}{2K(x)}$. Substituting these equalities in equation 4.11 the expansion for $v(x)$ can be written as,

$$v(x) = K(x) + i\frac{\epsilon K(x)'}{2K(x)} + \mathcal{O}(\epsilon^2). \tag{4.14}$$

Since we denoted $v(x) = u(x)'$, we integrate equation 4.14 once to get,

$$u(x) = \int_a^x K(\xi)d\xi + i\epsilon \int_a^x \frac{K(\xi)'}{2K(\xi)d\xi} + \mathcal{O}(\epsilon^2). \tag{4.15}$$

where a is an arbitrary constant and the other constants are incorporated into the indefinite integral. Using this expression for $u(x)$, we can obtain the expansion for $y(x)$ as,

$$\begin{aligned} y(x) &= e^{\left[\frac{i}{\epsilon}\left(\int_a^x K(\xi)d\xi + i\epsilon\int_a^x \frac{K'(\xi)}{2K(\xi)}d\xi\right)\right]} \\ &= e^{\left[\frac{i}{\epsilon}\int_a^x K(\xi)d\xi\right]}{}_e{}^{\left[\frac{i^2}{2}\int_a^x \frac{K'(\xi)}{K(\xi)}d\xi\right]} \\ &= e^{\left[\frac{i}{\epsilon}\int_a^x K(\xi)d\xi\right]}{}_e{}^{\ln\left(\frac{1}{k(x)^{\frac{1}{2}}}\right)} \\ &= \frac{1}{\sqrt{K(x)}} e^{\left[\frac{i}{\epsilon}\int_a^x K(\xi)d\xi\right]} \end{aligned} \tag{4.16}$$

Using the expression in equation 4.16, we can obtain the WKB approximation to the equation 4.8 in terms of sines and cosines as,

$$y_{wkb}(x) = \frac{1}{\sqrt{K(x)}}\left(c_1 \sin\left(\sqrt{\lambda}\int_0^x K(\xi)d\xi\right) + c_2\cos\left(\sqrt{\lambda}\int_0^x K(\xi)d\xi\right)\right). \tag{4.17}$$

where $\epsilon = \frac{1}{\sqrt{\lambda}}$ as previously noted.

4.4 OBTAINING THE EIGENVALUES

We can now try to solve for the eigenvalues of equation 4.17 with appropriate boundary conditions.

Specifically, $\Phi(0) = \Phi(2\pi)$ and $\Phi'(0) = \Phi'(2\pi)$ are the required boundary conditions. Since $y(x) = \Phi(x)G(x)$, and $K(x) = \sqrt{\frac{1}{G(x)}}$ we get,

$$\Phi(x) = K(x)^{\frac{3}{2}}\left(c_1 \sin\left(\sqrt{\lambda}\int_0^x K(\xi)d\xi\right) + c_2 \cos\left(\sqrt{\lambda}\int_0^x K(\xi)d\xi\right)\right). \tag{4.18}$$

The boundary conditions suggest that,

$$\begin{aligned}\Phi(0) &= K(0)^{\frac{3}{2}}\left(c_1 \sin\left(\sqrt{\lambda}\int_0^0 K(\xi)d\xi\right) + c_2 \cos\left(\sqrt{\lambda}\int_0^0 K(\xi)d\xi\right)\right) \\ &= c_2 K(0)^{\frac{3}{2}}\end{aligned} \tag{4.19}$$

Since, $G(x) = 1 - \frac{ch(x)}{h(0)}$ is a periodic function and given the boundary conditions $\Phi(0) = \Phi(2\pi)$, we can write,

$$\begin{aligned}\Phi(2\pi) &= K(2\pi)^{\frac{3}{2}}\left(c_1 \sin\left(\sqrt{\lambda}\int_0^{2\pi} K(\xi)d\xi\right) + c_2 \cos\left(\sqrt{\lambda}\int_0^{2\pi} K(\xi)d\xi\right)\right) \\ &= c_2 K(0)^{\frac{3}{2}}.\end{aligned} \tag{4.20}$$

Dividing both sides by $c_2 K(2\pi)^{\frac{3}{2}}$, we get the following equality,

$$\frac{c_1}{c_2} = \frac{1 - \cos\left(\sqrt{\lambda}\int_0^{2\pi} K(\xi)d\xi\right)}{\sin\left(\sqrt{\lambda}\int_0^{2\pi} K(\xi)d\xi\right)} \tag{4.21}$$

The boundary conditions $\Phi'(0) = \Phi'(2\pi)$ require differentiating under the integral sign with variable limits of integration using the Leibniz integral rule,

$$\frac{d}{d\alpha}\int_{a(\alpha)}^{b(\alpha)} f(x,\alpha)dx = \frac{db(\alpha)}{d\alpha}f(b\alpha,\alpha) - \frac{da(\alpha)}{d\alpha}f(a(\alpha),\alpha) + \int_{a(\alpha)}^{b(\alpha)} \frac{\partial}{\partial\alpha}f(x,\alpha)dx.$$

Using this rule, we can differentiate equation 4.18 to obtain,

$$\begin{aligned}\Phi'(x) = K(x)^{\frac{3}{2}}\Bigg(c_1\cos\left(\sqrt{\lambda}\int_0^x K(\xi)d\xi\right)\left[\sqrt{\lambda}\left(K(x)+\int_0^x K'(\xi)d\xi\right)\right] \\ - c_2\sin\left(\sqrt{\lambda}\int_0^x K(\xi)d\xi\right)\left[\sqrt{\lambda}\left(K(x)+\int_0^x K'(\xi)d\xi\right)\right]\Bigg).\end{aligned} \tag{4.22}$$

Using the boundary conditions $\Phi'(0) = \Phi'(2\pi)$ in equation 4.22 we get,

$$\begin{aligned}K(0)^{\frac{3}{2}}\left(c_1\sqrt{\lambda}K(0)\right) = K(2\pi)^{\frac{3}{2}}\Bigg(c_1\cos\left(\sqrt{\lambda}\int_0^{2\pi} K(\xi)d\xi\right)\left[\sqrt{\lambda}\left(K(2\pi)+\int_0^{2\pi} K'(\xi)d\xi\right)\right] \\ - c_2\sin\left(\sqrt{\lambda}\int_0^{2\pi} K(\xi)d\xi\right)\left[\sqrt{\lambda}\left(K(2\pi)+\int_0^{2\pi} K'(\xi)d\xi\right)\right]\Bigg)\end{aligned} \tag{4.23}$$

$$\begin{aligned}c_1\sqrt{\lambda}K(0) = c_1\cos\left(\sqrt{\lambda}\int_0^{2\pi} K(\xi)d\xi\right)\left[\sqrt{\lambda}\left(K(2\pi)+\int_0^{2\pi} K'(\xi)d\xi\right)\right] \\ - c_2\sin\left(\sqrt{\lambda}\int_0^{2\pi} K(\xi)d\xi\right)\left[\sqrt{\lambda}\left(K(2\pi)+\int_0^{2\pi} K'(\xi)d\xi\right)\right]\end{aligned} \tag{4.24}$$

Denoting $J = K(2\pi) + \int_0^{2\pi} K'(\xi)d\xi$, we can get the following equality,

$$\frac{c_1}{c_2} = \frac{\sin\left(\sqrt{\lambda}\int_0^{2\pi} K(\xi)d\xi\right)}{\cos\left(\sqrt{\lambda}\int_0^{2\pi} K(\xi)d\xi\right) - \frac{K(0)}{J}} \tag{4.25}$$

Denoting $H = \int_0^{2\pi} \sqrt{\lambda} K(\xi) d\xi$, we can use the equalities in equation 4.21 and 4.25 to obtain the following expression,

$$\sin^2(\sqrt{\lambda}H) = \cos(\sqrt{\lambda}H) - \cos^2(\sqrt{\lambda}H) + \frac{K(0)}{J}\cos(\sqrt{\lambda}H) - \frac{K(0)}{J}. \tag{4.26}$$

Using the trigonometric identity $\sin^2(x) + \cos^2(x) = 1$, we get,

$$1 = \cos(\sqrt{\lambda}H)\Big[1 + \frac{K(0)}{J}\Big] - \frac{K(0)}{J} \tag{4.27}$$

which simplifies to,

$$\cos(\sqrt{\lambda}H) = 1. \tag{4.28}$$

We can solve for λ in equation 4.28 as

$$\lambda = \frac{(n\pi)^2}{H^2} \tag{4.29}$$

where $n \in N$.

Thus we have successfully derived an expression for the eigenvalues.

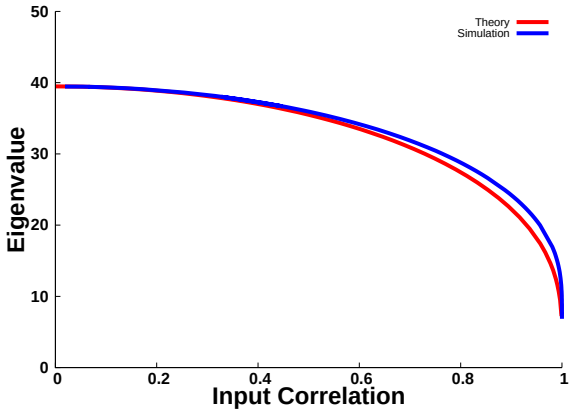

Figure 18: Second largest Eigenvalue for $c \in (0, 1)$

4.5 RESULTS

We plot the theoretically obtained eigenvalue corresponding to $n = 2$, to that obtained by numerical simulation in XPP [25] in figure 4.5 obtained at different values of input correlation. As can be observed the agreement between theory and simulation is good for large eigenvalues. But even for small values the agreement holds as a first approximation. Another observation is that lower the input correlation values, larger the eigenvalue. This can be accounted by the fact that at low input correlation values, the steady-state distribution can be well approximated by a uniform distribution. This means that if the systems with low input correlation starts with a uniform distribution, it is very close to its steady-state hence the convergence rates become almost instantaneous.

Interestingly, the rate of convergence depends on the PRC-type as shown in Figure 4.5. The plot shows simulation data using a parametrized PRC. Although, the absolute difference is not very significant, there is a definite minimum for the rate of convergence when the PRC is purely Type I. Hence Type II PRC's allow for faster rates of convergence than Type I.

Since both PING and stochastic synchrony mechanisms utilize the same inhibitory synapses, usual experimental manipulations involving inhibitory synaptic blockers do not provide a feasible experimental designs that could unequivocally eliminate one of the mechanisms.If

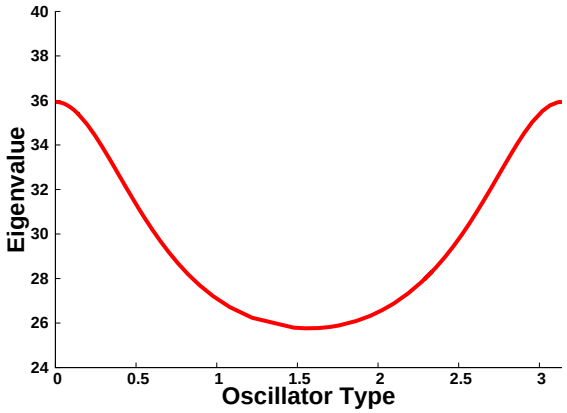

Figure 19: Second largest eigenvalue as a function of PRC-type at a fixed c.

the convergence rate for a single model incorporating both PING and stochastic synchrony are obtainable, it may be of use in comparing the two mechanisms experimentally since it introduces a measurable quantity that could be compared against predicted values which may assist in experimentally resolving the mechanism of synchrony in the olfactory bulb. A possibly simpler method would be investigate if there exists compounds that might be able shorten the mean latency of recruitment of the granule cell and sharpen the latency distribution. Even if the compound seat of action is not at the root cause of variable latency, it may be possible to discern specific changes in the function of the circuit from control to drug condition.

5.0 CONCLUSIONS

Here we list the main conclusions of this thesis.

1. We used perturbation methods to derive an expression relating the shape of the PRC to the probability density function of the phase difference between the oscillators. Our theory suggests that a Type-II PRC display a higher degree of synchronization using this mechanism compared to Type-I. We advise the reader that new results from our group suggest that on longer time-scales Type-I PRC's give a higher spike-count correlation.(Aushra Abouzeid, manuscript in preparation).
2. The degree of stochastic synchronization is controlled both by the firing rate of the neuron and the membership of the PRC (Type I or Type II).
3. The circular variance for the Leaky integrate-and-fire neuron and the generalized order parameter for a hippocampal interneuron model have a nonlinear relationship to the input correlation.
4. Increased synchrony in the mitral cells could produce an increase in granule cell activity for those granule cells that share a synchronous group of mitral cells. Common granule cell input increases the input correlation to the mitral cells and hence their synchrony by providing a positive feedback loop in correlation.
5. We demonstrate the emergence and temporal evolution of input correlation in recurrent networks with feedback. model.
6. We have obtained an expression that relates the rate of convergence of stochastic synchrony to the phase resetting curve.

BIBLIOGRAPHY

[1] Aushra Abouzeid and Bard Ermentrout. Type-ii phase resetting curve is optimal for stochastic synchrony. *Phys Rev E Stat Nonlin Soft Matter Phys*, 80(1 Pt 1):011911, Jul 2009.

[2] E. D. Adrian. Olfactory reactions in the brain of the hedgehog. *J Physiol*, 100(4):459–473, Mar 1941.

[3] E. D. Adrian. The electrical activity of the mammalian olfactory bulb. *Electroencephalogr Clin Neurophysiol*, 2(4):377–388, Nov 1950.

[4] E. D. Adrian and C. Ludwig. Nervous discharges from the olfactory organs of fish. *J Physiol*, 94(3):441–460, Dec 1938.

[5] F. H. Allen and O. Johnson. Automated conformational analysis from crystallographic data. 4. Statistical descriptors for a distribution of torsion angles. *Acta Crystallographica Section B*, 47(1):62–67, Feb 1991.

[6] Marlene Bartos, Imre Vida, and Peter Jonas. Synaptic mechanisms of synchronized gamma oscillations in inhibitory interneuron networks. *Nat Rev Neurosci*, 8(1):45–56, Jan 2007.

[7] Brice Bathellier, Samuel Lagier, Philippe Faure, and Pierre-Marie Lledo. Circuit properties generating gamma oscillations in a network model of the olfactory bulb. *J Neurophysiol*, 95(4):2678–2691, Apr 2006.

[8] Carl M. Bender and Steven A. Orszag. *Advanced Mathematical Methods for Scientists and Engineers: Asymptotic Methods and Perturbation Theory*. Springer-Verlag, Berlin, 1999.

[9] Christoph Borgers and Nancy Kopell. Synchronization in networks of excitatory and inhibitory neurons with sparse, random connectivity. *Neural Comput*, 15(3):509–538, Mar 2003.

[10] S. L. Bressler and W. J. Freeman. Frequency analysis of olfactory system eeg in cat, rabbit, and rat. *Electroencephalogr Clin Neurophysiol*, 50(1-2):19–24, Oct 1980.

[11] Eric Brown, Jeff Moehlis, and Philip Holmes. On the phase reduction and response dynamics of neural oscillator populations. *Neural Comput*, 16(4):673–715, Apr 2004.

[12] S.R.y. Cajal. Origen y terminacin de las fibras nerviosas olfatorias. *Gaceta Sanitaria de Barcelona.*, pages 133139, 174181, 206212., 1890.

[13] Jessica A Cardin, Marie Carln, Konstantinos Meletis, Ulf Knoblich, Feng Zhang, Karl Deisseroth, Li-Huei Tsai, and Christopher I Moore. Driving fast-spiking cells induces gamma rhythm and controls sensory responses. *Nature*, 459(7247):663–667, Jun 2009.

[14] G. C. Carlson, M. T. Shipley, and A. Keller. Long-lasting depolarizations in mitral cells of the rat olfactory bulb. *J Neurosci*, 20(5):2011–2021, Mar 2000.

[15] Jaime de la Rocha, Brent Doiron, Eric Shea-Brown, Kresimir Josic, and Alex Reyes. Correlation between neural spike trains increases with firing rate. *Nature*, 448(7155):802–806, Aug 2007.

[16] Brent Doiron, John Rinzel, and Alex Reyes. Stochastic synchronization in finite size spiking networks. *Phys Rev E Stat Nonlin Soft Matter Phys*, 74(3 Pt 1):030903, Sep 2006.

[17] R. Eckhorn, R. Bauer, W. Jordan, M. Brosch, W. Kruse, M. Munk, and H. J. Reitboeck. Coherent oscillations: a mechanism of feature linking in the visual cortex? multiple electrode and correlation analyses in the cat. *Biol Cybern*, 60(2):121–130, 1988.

[18] Veronica Egger and Nathaniel N Urban. Dynamic connectivity in the mitral cell-granule cell microcircuit. *Semin Cell Dev Biol*, 17(4):424–432, Aug 2006.

[19] C. Elton. Fluctuations in the numbers of animals: their causes and effects. *Br. J. Exp. Biol.*, 2:119163, 1924.

[20] A. K. Engel, P. Fries, and W. Singer. Dynamic predictions: oscillations and synchrony in top-down processing. *Nat Rev Neurosci*, 2(10):704–716, Oct 2001.

[21] B. Ermentrout. Type I membranes, phase resetting curves, and synchrony. *Neural Comput*, 8(5):979–1001, Jul 1996.

[22] B. Ermentrout and N. Kopell. *Handbook of Dynamical Systems*, volume 3. Elsevier, 2000.

[23] B. Ermentrout, M. Pascal, and B. Gutkin. The effects of spike frequency adaptation and negative feedback on the synchronization of neural oscillators. *Neural Comput*, 13(6):1285–1310, Jun 2001.

[24] Bard Ermentrout and David Saunders. Phase resetting and coupling of noisy neural oscillators. *J Comput Neurosci*, 20(2):179–190, Apr 2006.

[25] G. B. Ermentrout. *Simulating, Analyzing, and Animating Dynamical Systems: A Guide to XPPAUT for Researchers and Students*. SIAM, 2002.

[26] G. B. Ermentrout and N. Kopell. Fine structure of neural spiking and synchronization in the presence of conduction delays. *Proc Natl Acad Sci U S A*, 95(3):1259–1264, Feb 1998.

[27] G. Bard Ermentrout, Roberto F Galn, and Nathaniel N Urban. Reliability, synchrony and noise. *Trends Neurosci*, 31(8):428–434, Aug 2008.

[28] A. Fisahn, F. G. Pike, E. H. Buhl, and O. Paulsen. Cholinergic induction of network oscillations at 40 hz in the hippocampus in vitro. *Nature*, 394(6689):186–189, Jul 1998.

[29] W. J. Freeman. Measurement of oscillatory responses to electrical stimulation in olfactory bulb of cat. *J Neurophysiol*, 35(6):762–779, Nov 1972.

[30] Roberto F Galan, G. Bard Ermentrout, and Nathaniel N Urban. Efficient estimation of phase-resetting curves in real neurons and its significance for neural-network modeling. *Phys Rev Lett*, 94(15):158101, Apr 2005.

[31] Roberto F. Galan, G. Bard Ermentrout, and Nathaniel N. Urban. Reliability and stochastic synchronization in type i vs. type ii neural oscillators. *Neurocomputing*, 70:2102–2106, 2007.

[32] Roberto F. Galan, G. Bard Ermentrout, and Nathaniel N. Urban. Stochastic dynamics of uncoupled neural oscillators: Fokker-planck studies with the finite element method. *Phys Rev E Stat Nonlin Soft Matter Phys*, 76:056110, 2007.

[33] Roberto F Galan, Nicolas Fourcaud-Trocm, G. Bard Ermentrout, and Nathaniel N Urban. Correlation-induced synchronization of oscillations in olfactory bulb neurons. *J Neurosci*, 26(14):3646–3655, Apr 2006.

[34] Gillespie, D.T. Exact Stochastic Simulation of Coupled Chemical Reactions . *The Journal of Physical Chemistry*, 81:2340–2361, 1977.

[35] Joshua A Goldberg, Chris A Deister, and Charles J Wilson. Response properties and synchronization of rhythmically firing dendritic neurons. *J Neurophysiol*, 97(1):208–219, Jan 2007.

[36] Denis S Goldobin and Arkady Pikovsky. Synchronization and desynchronization of self-sustained oscillators by common noise. *Phys Rev E Stat Nonlin Soft Matter Phys*, 71(4 Pt 2):045201, Apr 2005.

[37] C. Golgi. Sulla fina struttura dei bulbi olfactorii,. *Riv. Sper. Freniatr. Med. Leg.*, 1:6678, 1875.

[38] D. Golomb and D. Hansel. The number of synaptic inputs and the synchrony of large, sparse neuronal networks. *Neural Comput*, 12(5):1095–1139, May 2000.

[39] C. M. Gray. Synchronous oscillations in neuronal systems: mechanisms and functions. *J Comput Neurosci*, 1(1-2):11–38, Jun 1994.

[40] C. M. Gray, P. Knig, A. K. Engel, and W. Singer. Oscillatory responses in cat visual cortex exhibit inter-columnar synchronization which reflects global stimulus properties. *Nature*, 338(6213):334–337, Mar 1989.

[41] C. M. Gray and W. Singer. Stimulus-specific neuronal oscillations in orientation columns of cat visual cortex. *Proc Natl Acad Sci U S A*, 86(5):1698–1702, Mar 1989.

[42] J. D. Green, M. Mancia, and von Baumgarten. Recurrent inhibition in the olfactory bulb. i. effects of antidromic stimulation of the lateral olfactory tract. *J Neurophysiol*, 25:467–488, Jul 1962.

[43] Boris S Gutkin, G. Bard Ermentrout, and Alex D Reyes. Phase-response curves give the responses of neurons to transient inputs. *J Neurophysiol*, 94(2):1623–1635, Aug 2005.

[44] D. Hansel, G. Mato, and C. Meunier. Synchrony in excitatory neural networks. *Neural Comput*, 7(2):307–337, Mar 1995.

[45] J. W. Hinds and P. L. Hinds. Synapse formation in the mouse olfactory bulb. i. quantitative studies. *J Comp Neurol*, 169(1):15–40, Sep 1976.

[46] Dawei Hong, William M Saidel, Shushuang Man, and Joseph V Martin. Extracellular noise-induced stochastic synchronization in heterogeneous quorum sensing network. *J Theor Biol*, 245(4):726–736, Apr 2007.

[47] J. S. Isaacson. Glutamate spillover mediates excitatory transmission in the rat olfactory bulb. *Neuron*, 23(2):377–384, Jun 1999.

[48] Vikrant Kapoor and Nathaniel N Urban. Glomerulus-specific, long-latency activity in the olfactory bulb granule cell network. *J Neurosci*, 26(45):11709–11719, Nov 2006.

[49] H. Kashiwadani, Y. F. Sasaki, N. Uchida, and K. Mori. Synchronized oscillatory discharges of mitral/tufted cells with different molecular receptive ranges in the rabbit olfactory bulb. *J Neurophysiol*, 82(4):1786–1792, Oct 1999.

[50] Leslie M Kay and Mark Stopfer. Information processing in the olfactory systems of insects and vertebrates. *Semin Cell Dev Biol*, 17(4):433–442, Aug 2006.

[51] James P. Keener. *Principles of Applied Mathematics: Transformation and Approximation*. Westview Press, 2000.

[52] Adam Kohn and Matthew A Smith. Stimulus dependence of neuronal correlation in primary visual cortex of the macaque. *J Neurosci*, 25(14):3661–3673, Apr 2005.

[53] Y. Kuramoto. *Chemical Oscillations, Waves and Turbulence*. New York: Springer Verlag, 1984.

[54] Y. Kuramoto. *Chemical oscillations, waves, and turbulence*, volume 19 of *Springer Series in Synergetics*. Springer-Verlag, Berlin, 1984.

[55] Samuel Lagier, Alan Carleton, and Pierre-Marie Lledo. Interplay between local gabaergic interneurons and relay neurons generates gamma oscillations in the rat olfactory bulb. *J Neurosci*, 24(18):4382–4392, May 2004.

[56] A. Lasota and M. C. Mackey. *Differential equations with applications to biology (Fields Institute Communications)*. Providence, RI : American Mathematical Society., 1999.

[57] Chunguang Li, Luonan Chen, and Kazuyuki Aihara. Stochastic synchronization of genetic oscillator networks. *BMC Syst Biol*, 1:6, 2007.

[58] Qianshu Li and Ying Wang. Coupling and internal noise sustain synchronized oscillation in calcium system. *Biophys Chem*, 129(1):23–28, Aug 2007.

[59] Jaime G Mancilla, Timothy J Lewis, David J Pinto, John Rinzel, and Barry W Connors. Synchronization of electrically coupled pairs of inhibitory interneurons in neocortex. *J Neurosci*, 27(8):2058–2073, Feb 2007.

[60] Sashi Marella and Bard Ermentrout. Amplification of asynchronous inhibition-mediated synchronization by feedback in recurrent networks. *PLoS Comput Biol*, 6(2):e1000679, 2010.

[61] Sashi Marella and G. Bard Ermentrout. Class-ii neurons display a higher degree of stochastic synchronization than class-i neurons. *Physical Review E (Statistical, Nonlinear, and Soft Matter Physics)*, 77:041918, 2008.

[62] Troy W Margrie and Andreas T Schaefer. Theta oscillation coupled spike latencies yield computational vigour in a mammalian sensory system. *J Physiol*, 546(Pt 2):363–374, Jan 2003.

[63] P.A.P. Moran. The statistical analysis of the canadian lynx cycle. ii synchronization and meteorology. *Aust. J. Zool.*, 1:291298, 1953.

[64] Rubn Moreno, Jaime de la Rocha, Alfonso Renart, and Nstor Parga. Response of spiking neurons to correlated inputs. *Phys Rev Lett*, 89(28 Pt 1):288101, Dec 2002.

[65] Hiroya Nakao, Ken-Suke Arai, Ken Nagai, Yasuhiro Tsubo, and Yoshiki Kuramoto. Synchrony of limit-cycle oscillators induced by random external impulses. *Phys Rev E Stat Nonlin Soft Matter Phys*, 72(2 Pt 2):026220, Aug 2005.

[66] Hiroya Nakao, Kensuke Arai, and Yoji Kawamura. Noise-induced synchronization and clustering in ensembles of uncoupled limit-cycle oscillators. *Phys Rev Lett*, 98(18):184101, May 2007.

[67] T.I. Netoff. Personal communication. personal communication.

[68] Z. Nusser, L. M. Kay, G. Laurent, G. E. Homanics, and I. Mody. Disruption of gaba(a) receptors on gabaergic interneurons leads to increased oscillatory power in the olfactory bulb network. *J Neurophysiol*, 86(6):2823–2833, Dec 2001.

[69] Kwangho Park, Ying-Cheng Lai, Satish Krishnamoorthy, and Anil Kandangath. Effect of common noise on phase synchronization in coupled chaotic oscillators. *Chaos*, 17(1):013105, Mar 2007.

[70] Benjamin Pfeuty, German Mato, David Golomb, and David Hansel. The combined effects of inhibitory and electrical synapses in synchrony. *Neural Comput*, 17(3):633–670, Mar 2005.

[71] Arkady Pikovsky, Michael Rosenblum, and Jrgen Kurths. *Synchronization: A Universal Concept in Nonlinear Sciences*. Cambridge University Press, 2003.

[72] A.S. Pikovsky. Synchronization and stochastization of the ensamble of autogenerators by external noise. *Radiophys.Quantum Electron*, 27, n.5:576–581, 1984.

[73] J. L. Price and T. P. Powell. The morphology of the granule cells of the olfactory bulb. *J Cell Sci*, 7(1):91–123, Jul 1970.

[74] J. L. Price and T. P. Powell. The synaptology of the granule cells of the olfactory bulb. *J Cell Sci*, 7(1):125–155, Jul 1970.

[75] W. Rall and G. M. Shepherd. Theoretical reconstruction of field potentials and dendrodendritic synaptic interactions in olfactory bulb. *J Neurophysiol*, 31(6):884–915, Nov 1968.

[76] W. Rall, G. M. Shepherd, T. S. Reese, and M. W. Brightman. Dendrodendritic synaptic pathway for inhibition in the olfactory bulb. *Exp Neurol*, 14(1):44–56, Jan 1966.

[77] Alex D Reyes. Synchrony-dependent propagation of firing rate in iteratively constructed networks in vitro. *Nat Neurosci*, 6(6):593–599, Jun 2003.

[78] J. Rinzel and G.B. Ermentrout. *Methods in Neuronal Modeling*. MIT Press, 1989.

[79] E. Salinas and T. J. Sejnowski. Correlated neuronal activity and the flow of neural information. *Nat Rev Neurosci*, 2(8):539–550, Aug 2001.

[80] N. E. Schoppa, J. M. Kinzie, Y. Sahara, T. P. Segerson, and G. L. Westbrook. Dendrodendritic inhibition in the olfactory bulb is driven by nmda receptors. *J Neurosci*, 18(17):6790–6802, Sep 1998.

[81] N. E. Schoppa and G. L. Westbrook. Glomerulus-specific synchronization of mitral cells in the olfactory bulb. *Neuron*, 31(4):639–651, Aug 2001.

[82] Nathan E Schoppa. Synchronization of olfactory bulb mitral cells by precisely timed inhibitory inputs. *Neuron*, 49(2):271–283, Jan 2006.

[83] Nathan E Schoppa and Nathan N Urban. Dendritic processing within olfactory bulb circuits. *Trends Neurosci*, 26(9):501–506, Sep 2003.

[84] G.M. Shepherd and C.A. Greer. *Olfactory bulb. In The Synaptic Organization of the Brain.* New York:Oxford UP, 1998.

[85] Gordon M Shepherd, Wei R Chen, David Willhite, Michele Migliore, and Charles A Greer. The olfactory granule cell: from classical enigma to central role in olfactory processing. *Brain Res Rev*, 55(2):373–382, Oct 2007.

[86] W. Singer. Neuronal synchrony: a versatile code for the definition of relations? *Neuron*, 24(1):49–65, 111–25, Sep 1999.

[87] W. Singer and C. M. Gray. Visual feature integration and the temporal correlation hypothesis. *Annu Rev Neurosci*, 18:555–586, 1995.

[88] Vikaas S Sohal, Feng Zhang, Ofer Yizhar, and Karl Deisseroth. Parvalbumin neurons and gamma rhythms enhance cortical circuit performance. *Nature*, 459(7247):698–702, Jun 2009.

[89] M. Stopfer, S. Bhagavan, B. H. Smith, and G. Laurent. Impaired odour discrimination on desynchronization of odour-encoding neural assemblies. *Nature*, 390(6655):70–74, Nov 1997.

[90] G. Tams, P. Somogyi, and E. H. Buhl. Differentially interconnected networks of gabaergic interneurons in the visual cortex of the cat. *J Neurosci*, 18(11):4255–4270, Jun 1998.

[91] T. Tateno and H. P C Robinson. Phase resetting curves and oscillatory stability in interneurons of rat somatosensory cortex. *Biophys J*, 92(2):683–695, Jan 2007.

[92] T. Tateno and H. P C Robinson. Quantifying noise-induced stability of a cortical fast-spiking cell model with kv3-channel-like current. *Biosystems*, 89(1-3):110–116, 2007.

[93] Jun-Nosuke Teramae and Dan Tanaka. Robustness of the noise-induced phase synchronization in a general class of limit cycle oscillators. *Phys Rev Lett*, 93(20):204103, Nov 2004.

[94] P. H E Tiesinga and T. J. Sejnowski. Rapid temporal modulation of synchrony by competition in cortical interneuron networks. *Neural Comput*, 16(2):251–275, Feb 2004.

[95] R. D. Traub, M. A. Whittington, S. B. Colling, G. Buzsaki, and J. G. Jefferys. Analysis of gamma rhythms in the rat hippocampus in vitro and in vivo. *J Physiol*, 493 (Pt 2):471–484, Jun 1996.

[96] R. D. Traub, M. A. Whittington, I. M. Stanford, and J. G. Jefferys. A mechanism for generation of long-range synchronous fast oscillations in the cortex. *Nature*, 383(6601):621–624, Oct 1996.

[97] Yasuhiro Tsubo, Masahiko Takada, Alex D Reyes, and Tomoki Fukai. Layer and frequency dependencies of phase response properties of pyramidal neurons in rat motor cortex. *Eur J Neurosci*, 25(11):3429–3441, Jun 2007.

[98] Nathaniel N Urban and Bert Sakmann. Reciprocal intraglomerular excitation and intra- and interglomerular lateral inhibition between mouse olfactory bulb mitral cells. *J Physiol*, 542(Pt 2):355–367, Jul 2002.

[99] Imre Vida, Marlene Bartos, and Peter Jonas. Shunting inhibition improves robustness of gamma oscillations in hippocampal interneuron networks by homogenizing firing rates. *Neuron*, 49(1):107–117, Jan 2006.

[100] C. Van Vreeswijk, L. F. Abbott, and G. B. Ermentrout. When inhibition not excitation synchronizes neural firing. *J Comput Neurosci*, 1(4):313–321, Dec 1994.

[101] X. J. Wang and G. Buzsaki. Gamma oscillation by synaptic inhibition in a hippocampal interneuronal network model. *J Neurosci*, 16(20):6402–6413, Oct 1996.

[102] X. J. Wang and J. Rinzel. Spindle rhythmicity in the reticularis thalami nucleus: synchronization among mutually inhibitory neurons. *Neuroscience*, 53(4):899–904, Apr 1993.

[103] M. A. Whittington, J. G. Jefferys, and R. D. Traub. Effects of intravenous anaesthetic agents on fast inhibitory oscillations in the rat hippocampus in vitro. *Br J Pharmacol*, 118(8):1977–1986, Aug 1996.

[104] M. A. Whittington, I. M. Stanford, S. B. Colling, J. G. Jefferys, and R. D. Traub. Spatiotemporal patterns of gamma frequency oscillations tetanically induced in the rat hippocampal slice. *J Physiol*, 502 (Pt 3):591–607, Aug 1997.

[105] M. A. Whittington, R. D. Traub, and J. G. Jefferys. Synchronized oscillations in interneuron networks driven by metabotropic glutamate receptor activation. *Nature*, 373(6515):612–615, Feb 1995.

[106] David C Willhite, Katherine T Nguyen, Arjun V Masurkar, Charles A Greer, Gordon M Shepherd, and Wei R Chen. Viral tracing identifies distributed columnar organization in the olfactory bulb. *Proc Natl Acad Sci U S A*, 103(33):12592–12597, Aug 2006.

[107] Wenhui Xiong and Wei R Chen. Dynamic gating of spike propagation in the mitral cell lateral dendrites. *Neuron*, 34(1):115–126, Mar 2002.

[108] Kazuyuki Yoshimura, Ingrida Valiusaityte, and Peter Davis. Synchronization induced by common colored noise in limit cycle and chaotic systems. *Phys Rev E Stat Nonlin Soft Matter Phys*, 75(2 Pt 2):026208, Feb 2007.